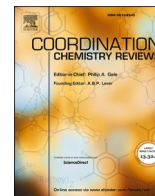




Contents lists available at ScienceDirect

## Coordination Chemistry Reviews

journal homepage: [www.elsevier.com/locate/ccr](http://www.elsevier.com/locate/ccr)

## Advancements and synthetic strategies in conjugated covalent organic cages

Jiajia Li<sup>a,b,1</sup>, Yanping Yang<sup>a,b,1</sup>, Jinghui Yang<sup>c,1</sup>, Cheng Huang<sup>a</sup>, Xinyuan Zhu<sup>a</sup>, Youfu Wang<sup>a,\*</sup>

<sup>a</sup> School of Chemistry and Chemical Engineering, Shanghai Jiao Tong University, Shanghai 200240, China

<sup>b</sup> School of Materials Engineering, Shanghai University of Engineering Science, Shanghai 201620, China

<sup>c</sup> Department of Organ Transplantation, Shanghai Changzheng Hospital, Naval Medical University, Shanghai 200003, China

## ARTICLE INFO

## Keywords:

Conjugation

Covalent organic cage

Aromaticity

Host-guest interaction

## ABSTRACT

Conjugated covalent organic cages (cCOCs) are three-dimensional (3D) giant molecules characterized by  $\pi$ -conjugated skeletons and interconnected multi-windows. Their atomically precise and stable structures, combined with intriguing optoelectronic properties, have garnered significant attention for interpreting aromaticity and exploring host-guest interactions. However, a critical limitation of cCOCs is the challenge of synthesizing them with on-demand compositions, topologies, sizes, functionalities, and properties. This difficulty arises from high strain barriers and complex synthetic processes that often yield low outputs. In the past decade, various synthetic strategies have been developed to address these challenges. In this review, we first categorize cCOCs into four distinct classes based on the nature of their bridging fragments. We then provide a comprehensive overview of recent advancements in the rational bottom-up synthesis of 3D cCOCs, along with insights into their aromaticity and host-guest interactions. Finally, we discuss the current challenges and future directions for cCOCs, particularly in the context of novel optoelectronic applications.

### 1. Introduction

Conjugated systems with delocalized electrons exhibit intriguing optoelectronic properties [1–4], which have extensive applications in imaging [5,6], sensing [7,8], energy conversion [9,10] and storage [3,4], and optoelectronics [11]. These systems encompass a variety of structures, including small molecules, nanocarbons (fullerene, carbon nanotube, graphene, etc.) [8,12–14], and polymers (including COFs, MOFs) [15–18]. They have significantly contributed to scientific advancements and technological innovations that enhance human well-being. However, conjugated small molecules and certain nanocarbons often suffer from low solubility and poor processability due to strong  $\pi$ - $\pi$  interactions [6,14,19]. In contrast, conjugated polymers may display heterogeneous properties arising from their flexible and imprecise structures [5,6]. Therefore, there is a pressing need for conjugated systems that possess precise structures and minimal  $\pi$ - $\pi$  stacking tendencies. Conjugated systems with three-dimensional (3D) curved skeletons show considerable promise as potential candidates, given their excellent stability, shape persistence, adjustable porosity, and solubility in common solvents [20–24]. Among these, conjugated covalent organic

cages (cCOCs) have emerged as a noteworthy category of 3D carbon-rich nanoobjects. cCOCs possess unique structural characteristics, including curved and rigid skeletons, atomic precision, outstanding stability, accessible cavities, globally delocalized electrons, and remarkable photophysical properties [20,23,25–36].

The synthesis of cCOCs holds significant importance in supramolecular chemistry and nanotechnology due to their distinctive structural features and diverse functionalities. These properties make cCOCs highly desirable for various applications, including drug delivery [37–40], biomolecular sensing [20,21,25,27,30,41,42], and the development of nanoscale devices [30,37,38,43,44]. Furthermore, advancements in cCOC synthesis enhance our understanding of fundamental principles in supramolecular chemistry and pave the way for innovative designs and productions of functional molecular structures. By elucidating the synthetic strategies and techniques for cCOC creation, researchers can leverage the exceptional properties of these complex molecules to address various challenges in biomedicine and materials science. Additionally, cCOCs are vital for interpreting aromaticity [28,29,35,45–49] and host-guest interactions [26,27,32,46,50,51] owing to their unique conjugated characteristics and cavity structures.

\* Corresponding author.

E-mail address: [wfyf@sjtu.edu.cn](mailto:wfyf@sjtu.edu.cn) (Y. Wang).

<sup>1</sup> Jiajia Li, Yanping Yang and Jinghui Yang contributed equally to this work.

<https://doi.org/10.1016/j.ccr.2024.216260>

Received 20 August 2024; Received in revised form 28 September 2024; Accepted 30 September 2024

0010-8545/© 2024 Elsevier B.V. All rights are reserved, including those for text and data mining, AI training, and similar technologies.

Since 1977, chemists have pursued the development of hydrocarbon-based cCOCs that bridge through double and triple bonds utilizing various carbon-carbon coupling reactions [34,45,52–56]. Current conventional methods primarily involve reversible alkyne metathesis [32] and irreversible transition metal-mediated coupling reactions [22] to form conjugated covalent bonds for cCOC synthesis. However, these synthetic approaches present challenges, including multi-step processes, the need for pre-organization of building blocks, a lack of general methodologies, low overall yields, and difficulties in preparing cCOCs with higher strain [57]. The principal limitation in the development of cCOCs lies in the challenges associated with effectively tailoring their compositions, topologies, sizes, functionalities, and properties. These challenges stem from the high strain barriers and the complexities of synthetic processes that often result in low yields.

To address these challenges, the bottom-up chemical synthesis strategies offer promising avenues for the preparation of cCOCs with high purity and yield [20,22,25,32,36,37,41,48,58,59]. From a structural perspective, cCOCs can be categorized into four groups based on their bridging units: single bonds, double bonds, triple bonds, and single atoms. Thanks to the dedicated efforts of numerous scientists, significant advancements have been made over the past decade in the synthetic strategies and property studies of cCOCs. Various innovative synthetic approaches have been developed to obtain cCOCs with diverse structures (Fig. 1). In this review, we first categorize cCOCs into four distinct classes based on the nature of their bridging fragments. We then provide a comprehensive overview of recent progress in the rational bottom-up synthesis of 3D cCOCs, alongside an exploration of their aromaticity and host-guest interactions. By elucidating recent advancements in synthetic methodologies for cCOCs, we aim to enhance understanding of the challenges and opportunities in advancing the chemistry of cCOCs in the future.

## 2. All-aryl cCOCs

The all-aryl cCOCs are 3D structures exclusively composed of all-carbon aryl or heterocycle linked solely through C–C single bonds. These unique architectures offer significant potential in host-guest chemistry and organic electronics due to their previously undiscovered

symmetrical arrangements combining linear and branched aryl blocks [21–25,41,60]. The synthesis of these cages represents ongoing efforts to develop curved  $\pi$ -conjugated systems with enclosed 3D architectures, similar to fullerenes and carbon nanotubes [61–63]. However, the fabrication of such strained and conjugated cages poses notable challenges. The primary obstacles stem from the substantial strain energy that arises during the synthetic process, as well as the need for effective component-assembling strategies [20–22,41]. Currently, all-aryl cCOCs can be categorized into two groups: all-carbon all-aryl cCOCs and heteroatomic all-aryl cCOCs.

### 2.1. All-carbon all-aryl cCOCs

The construction of all-carbon all-aryl cCOCs draws inspiration from their analogues, cycloparaphenylenes (CPPs) [62,64–66]. Comprising cyclic all-*para*-linked phenyl groups, [n]CPPs (n, the number of benzene rings) are hoop-shaped, highly strained conjugated molecules that serve as the basic structural unit of armchair carbon nanotubes [67–69]. Since their inception in 2008, CPPs have seen a remarkable surge due to their intriguing properties, including size-dependent photophysical characteristics [61,62,66,70,71] and host-guest capabilities [72,73], as well as their potential in constructing carbon nanoobjects [74–76]. The synthesis and expansion of CPPs have significantly enhanced our understanding of aromaticity and conjugation in physical organic chemistry, providing valuable insights into the construction of 3D all-aryl cCOCs. There are generally three main strategies employed to construct all-carbon all-aryl cCOCs: aromatization of strain buffers, metal templating, and multiple coupling. Several strain-buffering groups have been utilized to effectively mitigate the challenges posed by the high strain energy during the synthesis of these curved aromatic structures. Examples include 3,6-*syn*-dimethoxy-cyclohexa-1,4-diene [20,24,60], *cis*-1,4-diphenylcyclohexane [21,77,78], and ethylene moiety [41], which serve as strain-buffering components. These groups not only help reduce strain but also incorporate concealed aromatic rings, facilitating the preparation of cage precursors that ultimately yield all-aryl cCOCs after aromatization (Fig. 2A–C). Additionally, an angled *cis*-platinum linkage has been employed as a metal template, acting as corners to form rigid cage precursors. These precursors can then undergo reductive elimination to produce the final all-aryl cCOCs (Fig. 2D) [22]. Alternatively, direct multiple coupling of functional flexible or twisted blocks can also be effectively utilized to obtain all-aryl cCOCs (Fig. 2E) [23,25].

In 2013 and 2014, Prof. Itami successfully expanded CPPs to [n.n.n]COCs, specifically COC-1 ( $n = 4$ ), COC-2 ( $n = 5$ ), and COC-3 ( $n = 6$ ), employing strategy A for the first time [20,60]. Similar to the synthesis of [14]–[16]CPPs, a triangular prism-like cage precursor (2) was synthesized, featuring six L-shaped strain-buffering moieties. This precursor was obtained via a three-fold Ni(0)-mediated Yamamoto coupling reaction, utilizing cyclohexane derivatives as corners and two benzene

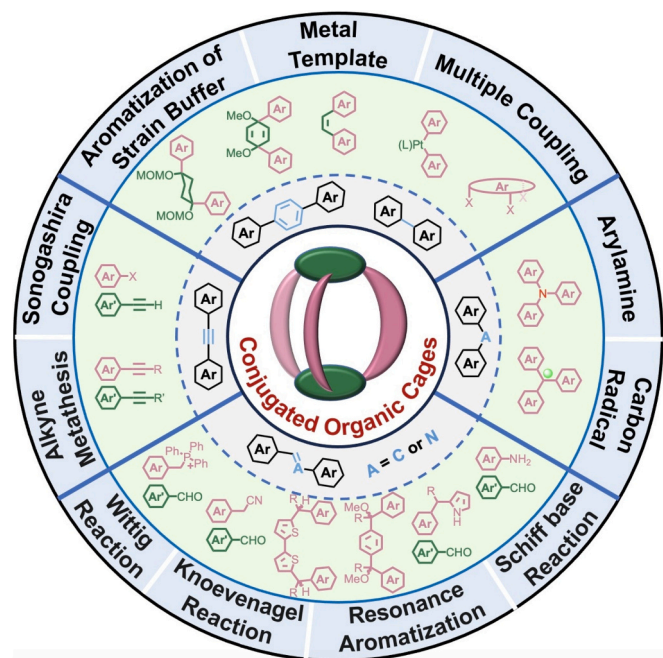


Fig. 1. Summary of synthetic approaches for the synthesis of cCOCs with different bridging fragments.

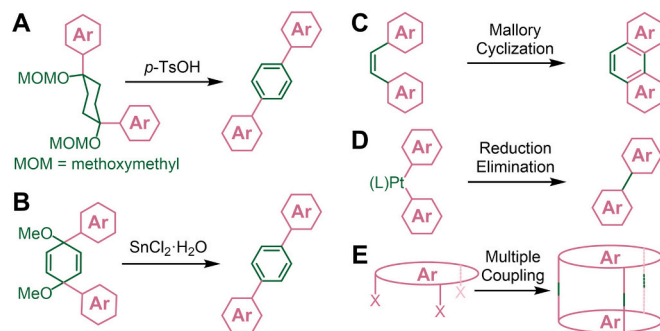


Fig. 2. Synthetic approaches for all-carbon all-aryl cCOCs. Aromatization of strain-buffering groups, (A) 3,6-*syn*-dimethoxy-cyclohexa-1,4-diene, (B) *cis*-1,4-diphenylcyclohexane, and (C) ethylene. (D) Metal templating followed by reductive elimination. (E) Multiple coupling of multifunctional precursors.

cores [60]. The subsequent aromatization of these corners enabled to the successful preparation of **COC-3** with twenty benzene units (Fig. 3A). In order to address the increased strain energies observed in smaller cCOC precursors, a novel L-shaped strain-buffering component, 4-(4-chlorophenyl)-4-hydroxycyclohexan-1-one (**3**), was designed. The trifurcate units (**4**, **5** and **6**) were synthesized from this innovative cyclohexane unit. Through the multiple coupling reaction ( $4 + 4$ ,  $4 + 5$ , and  $5 + 6$ ), cage precursors containing cyclohexane moiety were successfully obtained (Fig. 3B). **COC-1** and **COC-2** were then synthesized through the aromatization transformation from cyclohexane to benzene. Single crystal X-ray diffraction (SC-XRD) analysis of **COC-1** confirms the cage-like architecture, complete with a spherical void [20,60]. The sizes of the [n.n.n]COCs are situated within the ranges defined by their corresponding  $[2n + 1]$ CPPs and  $[2n + 2]$ CPPs. Notably, as the size of these cCOCs increases, they exhibit red-shifted absorption and blue-shifted emission maxima, which can be attributed to the orbital interactions between the three *para*-phenylene arms and the two benzene bridge-heads. Furthermore, all aforementioned cCOCs display intense blue fluorescence, with high fluorescence quantum yields of 0.66, 0.76, and 0.87 for **COC-1**, **COC-2**, and **COC-3**, respectively. The unique characteristics of these cCOCs—including strain energy, size-dependent absorption, fluorescence behavior, and electronic features—render them particularly attractive alongside their innovative synthetic strategy.

To enhance the conjugation of all-aryl cCOCs, hexa-*peri*-hexabenzocoronene (HBC) was employed as a bridgehead to replace benzene in the construction of **COC-3-HBC** [24]. Using C–H borylation and Suzuki–Miyaura cross-coupling reaction, Prof. Du successfully synthesized bromic HBC with cyclohexane, which was then utilized in a triple Yamamoto coupling and following aromatization of the cyclohexane units to prepare **COC-3-HBC** (Fig. 3C). As a larger conjugated block, HBC increases the conjugation degree and enhances the structural rigidity of **COC-3-HBC** [24,79]. The absorption peaks of **COC-3-HBC** (374, 358, and 408 nm) exhibit a significant redshift compared to those of **COC-3** (325 nm) and trimesityltriphenyl-HBC. In dichloromethane at room temperature, **COC-3-HBC** displays intense green photoluminescence, characterized by multiple emission peaks at 480, 503, and 536 nm when excited at 350 nm. The cage demonstrates a fluorescence quantum yield of  $\Phi_F = 17.1\%$  and an enhanced fluorescence lifetime of 16.1 ns, in contrast to 1.4 ns for **COC-3** and 2.1 ns for the subsequent ball-like **COC-5** [22]. The cage-like structure of **COC-3-HBC**, featuring a cavity of approximately 10.5 Å, can serve as a supramolecular host for conjugated convex molecules such as fullerenes, and exhibits strong supramolecular interaction with  $C_{70}$ . Investigations into host-guest behavior reveal that **COC-3-HBC** can form a 1:1 complex with  $C_{70}$ , with a binding constant of approximately  $1.0 \times 10^5 \text{ M}^{-1}$ , as determined through UV–vis and fluorescence titration experiments.

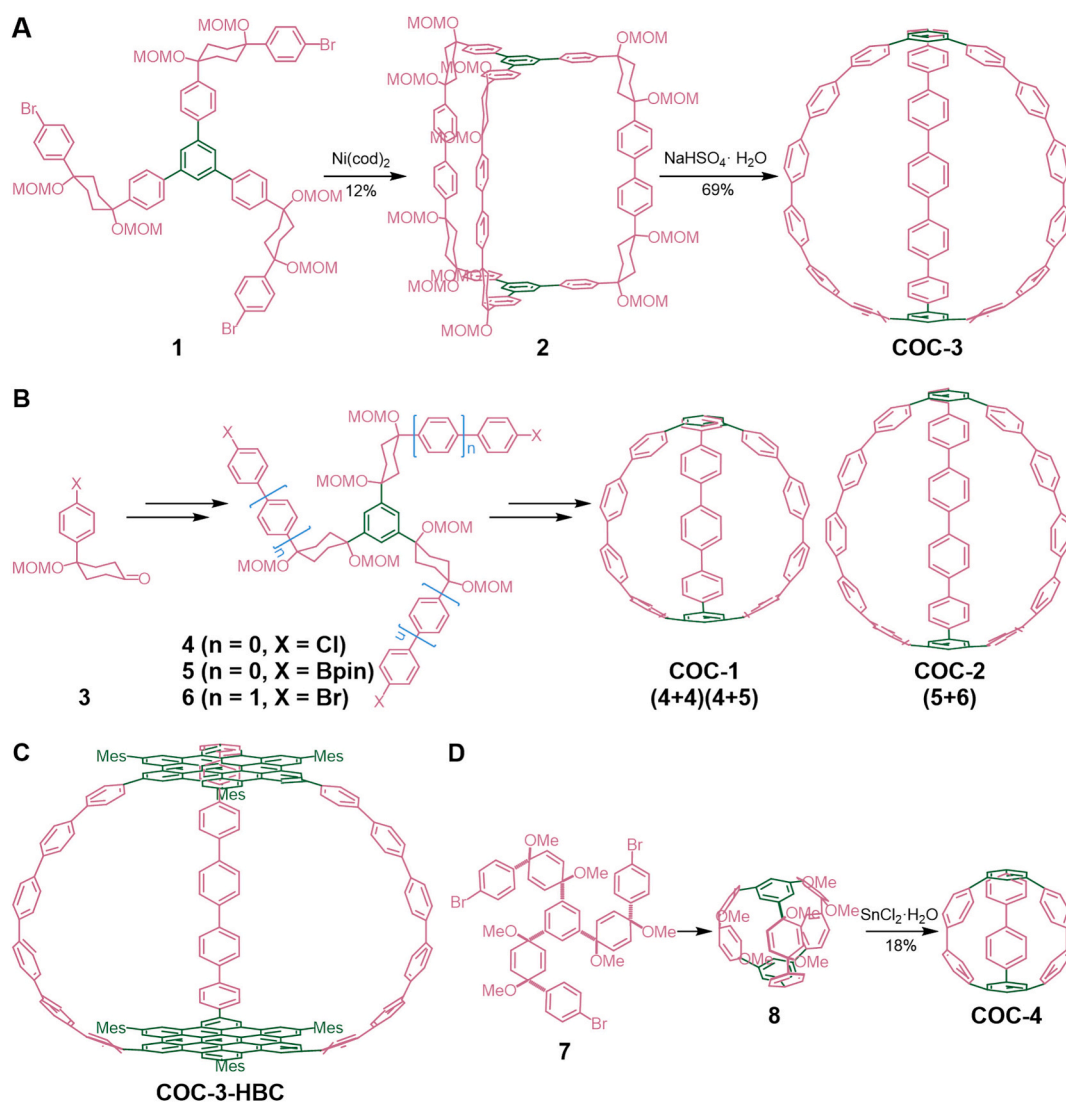


Fig. 3. Synthetic approaches and structures of [n.n.n]COCs, **COC-1** ~ **COC-4**.

Despite the high conformational flexibility of 3,6-*syn*-dimethoxycyclohexa-1,4-diene, the cyclohexane template encounters significant challenges in achieving aromatization due to high strain energy, complicating the synthesis of smaller cCOCs with increased strain [75,80,81]. In 2018, Tanaka successfully synthesized the smallest spherical [2.2.2]COC, **COC-4**, by employing cyclohexadiene as a strain-buffering component to provide the necessary rigidity and curvature for cage precursors (Fig. 3D) [21]. Highly strained **COC-4** can be synthesized effectively through triple Suzuki–Miyaura cross-coupling reaction, followed by reductive aromatization of the cyclohexadiene moieties. This cage exhibits a notable blue-shift in its absorption maximum at 302 nm and a red-shift in its emission maximum at 499 nm, compared to **COC-1** ( $\lambda_{ab} = 316$  nm,  $\lambda_{em} = 427$  nm). However, attempts to synthesize the even smaller spherical [1.1.1]COC using the same methodology was unsuccessful due to the significantly higher curvature requirements for the cage precursor.

The formation of a covalent platinum complex with an aryl group through the transmetalation process of arylmetal reagents and a platinum halide, followed by reductive elimination of platinum, represents an effective strategy for constructing CPP [82–84]. Inspired by this approach, an octahedral precursor (**9**) featuring hexanuclear platinum was synthesized through a twelve-fold stannane–platinum transmetalation process. The platinum component was subsequently eliminated via a six-fold reduction process, resulting in the formation of spherical **COC-5** (Fig. 4) [22]. The reductive elimination of the *cis*-substituted platinum complex, characterized by an ideal bond angle close to 90°, converted a strain-free metal complex precursor into a highly strained cCOC. Two reductive agents were utilized to complete this process with yields of approximately 20 % for XeF<sub>2</sub> or PPh<sub>3</sub>. The calculated strain energy of **COC-5** is 501 kJ·mol<sup>-1</sup>, exceeding that of both [6]CPP (407 kJ·mol<sup>-1</sup>) and [5]CPP (491 kJ·mol<sup>-1</sup>). Crystal structure analysis reveals that within a single body-centered quasi-cubic geometry, the central **COC-5** is encircled by eight neighboring vertices. Additionally, weak offset C–H/ $\pi$  interactions between the central and vertex **COC-5** contribute to high charge mobility and moderate hole mobility ( $3.0 \times 10^{-3}$  cm<sup>2</sup>·V<sup>-1</sup>·s<sup>-1</sup>), indicating its potential as a material for charge transport in molecular electronics.

The ethylene moiety has been employed as a strain-buffering component in the construction of conjugated macrocycles and cCOCs via Mallory cyclization [85–87]. Prof. Durola successfully synthesized a novel chiral cage, **COC-6**, which features helicene moieties as arms and exhibits a triple macrocycle with a rigid, propeller-shaped conjugated structure [41]. To create such a strained cage, flexible precursors (**12**) containing aromatic fragments connected by maleic (diester [86] or imide [88]) moieties were targeted through Perkin reaction involving arylacetic and arylglyoxylic acids. The resultant **COC-6** was then rigidified through a six-fold Mallory cyclization, facilitated by the presence of light, iodine, and oxygen (Fig. 5). This synthetic strategy encompasses a complex three-fold Perkin olefination followed by Mallory cyclization, effectively demonstrating the method's capacity to generate highly

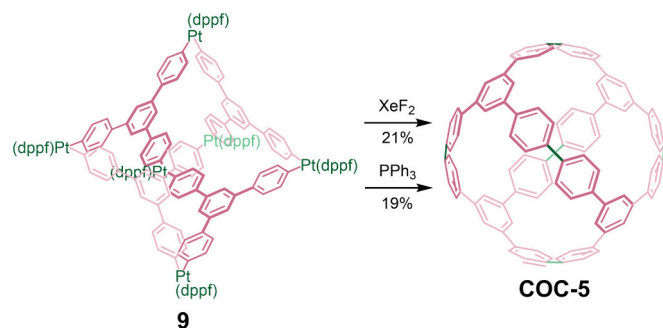


Fig. 4. Spherical all-aryl **COC-5** through the reductive elimination of hexanuclear aryl platinum complex as precursor.

restricted structures. Moreover, initial computational simulations of chiral **COC-6** suggest a highly inflexible *D*<sub>3</sub> symmetry, characterized by perfectly stacked central benzene rings separated by a distance of 3.6 Å. This close arrangement, along with the overall rigidity of the structure, may enhance its aromaticity, thereby significantly advancing research on global aromaticity in 3D cCOCs.

Given the considerable challenges associated with synthesizing closed and twisted polycyclic aromatic hydrocarbons (PAHs) featuring fused ring systems, Watanabe's group concentrated on three-fold symmetrical multiple helicenes, particularly the thermodynamically stable triple [5]helicene. This molecule is characterized by three functional groups located at the terminal ends of the outer fraction, all positioned on one side [25]. Watanabe successfully synthesized a chiral triple helicene cage, **COC-7**, through the dimerization of triflate-substituted triple [5]helicene (**14**) via Yamamoto coupling (Fig. 6). Crystal analysis reveals that **COC-7**, which comprises twenty benzene rings and six [5]helicene units, exhibits a rigid, cage-like structure with spiral grooves on the exterior and a chiral cavity within. Furthermore, photoelectric investigations of **COC-7** demonstrate a low fluorescence quantum yield of 0.017, which is comparable to that of triple [5]helicene ( $\Phi_F = 0.026$ ).

In 2018, Krische proposed an innovative strategy for constructing helical rod-like cCOCs through the three-fold homocoupling of tripodal *p*-bromo-terminated oligo-(phenylenes) (**15a** and **15b**), which were synthesized via diene-diol benzannulation [23]. The resulting compounds, **COC-8** ~ **COC-10**, feature triple-stranded phenylene structures containing fourteen, seventeen, and twenty benzene rings, respectively (Fig. 7). As the number of benzene rings increases, a progressively red-shifted emission of these cCOCs is observed in these cCOCs, indicating an extension of the conjugated degree that enhances emission. Notably, this red shift is not uniformly mirrored in the absorption spectra; for instance, **COC-9**, which has an intermediate size, displays a blue-shifted absorption maximum compared to the smaller **COC-8**. This intriguing observation adds another highlight to this work in addition to the synthesis strategy. Understanding the physical origin of this absorption trend will pave the way for leveraging these spiral rod benzene cages in the development of advanced organic optoelectronic materials.

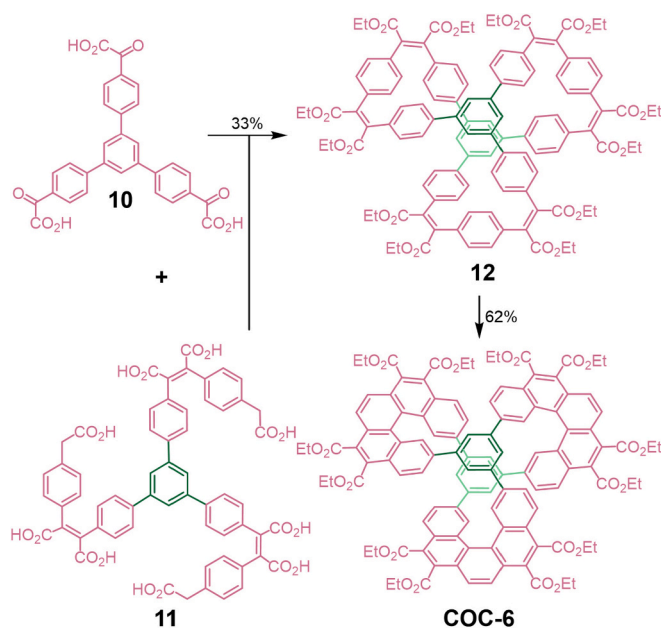


Fig. 5. Synthesis of [5]helicene-bridged **COC-6** via Perkin reaction and Mallory photocyclization.

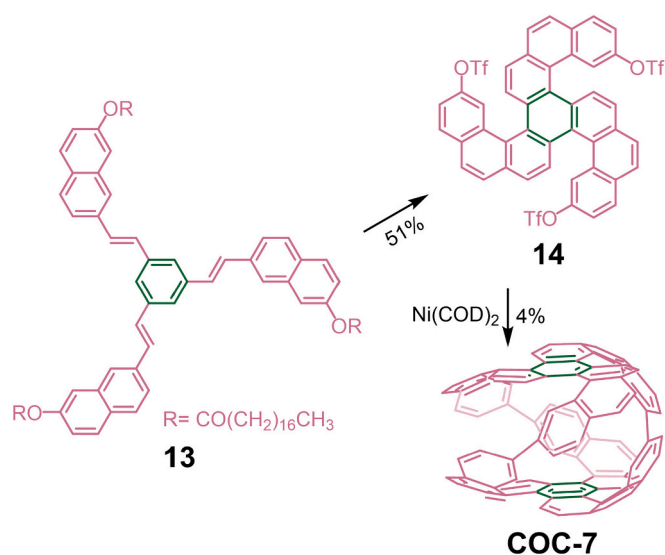


Fig. 6. Synthesis of triple [5]helicene-capped COC-7 via oxidative photocyclization and multiple Yamamoto coupling reaction.

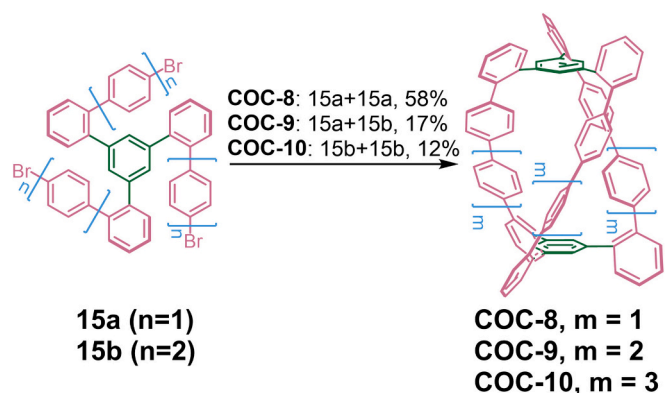


Fig. 7. Helical rod-like COC-8 ~ COC-10 synthesized through three-fold homocoupling reaction.

## 2.2. Heterocycle all-aryl cCOCs

The integration of hydrocarbon cages with heteroatoms has led to the emergence of a new category of carbon nanomaterials, characterized by unique properties and diverse applications [26]. When thiophene-containing heterocyclic units introduce steric hindrance, they can facilitate the formation of cage-like  $\pi$ -conjugated systems, effectively displacing macrocycles [27,46,58]. This approach not only enhances the yield of pre-metallic porphyrin cages but also contributes to development of 3D distorted  $\pi$  conjugation system [27]. Furthermore, the nitrogen donor core in pyridine groups or porphyrins can coordinate with metal ions, enabling interactions within cCOCs' cavity beyond simple metal cation complexation [26]. This feature is particularly advantageous for the design of functional cCOCs with larger internal and external cavities or for more extensive cCOC-based systems. In 2019, Dr. Krische successfully utilized three-fold Suzuki cross coupling of **16** and **17** to synthesize racemic triple helical N-doped cCOC, **COC-11**. Subsequently, **COC-11** was metallized with  $\text{Ir}(\text{acac})_3$  to yield conformationally restricted **Ir-COC-11** (Fig. 8) [89]. Interestingly, while **COC-11** exhibits high solubility in halogenated solvents, the metallized **Ir-COC-11** displays limited solubility due to a reduction in conformational mobility. Nevertheless, **Ir-COC-11** preserves the optical characteristics of *fac*- $\text{Ir}(\text{PPy})_3$  parent complex, demonstrating an elevated phosphorescence quantum yield, substantial Stoke shifts, and exceptional

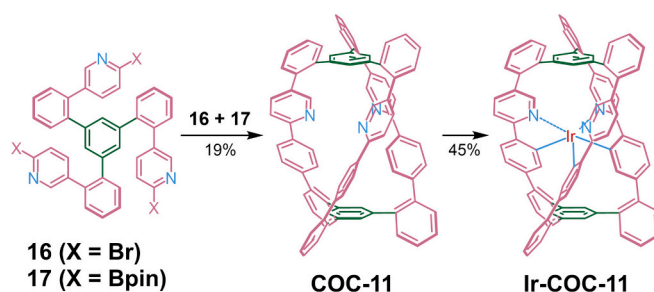


Fig. 8. Helical rod-like N-doped COC-11 and its metallized Ir-COC-11.

chemical and thermal photostability. These findings significantly broaden the scope of chiral cCOCs and enhance their potential applications in optical luminescence.

In 2010, Aratani's study on the  $\beta,\beta'$ -doubly 2,6-pyridylene-bridged Ni(II)-porphyrin cage, **COC-12**, marked a significant advancement in the field of heteroatomic cCOCs [26]. Porphyrin, a prototypical planar and aromatic macrocycle, exhibits structural and electrical flexibility dependent on steric hindrance and peripheral substitution. This adaptability can be further exploited through pronounced bending or distortion. However, it is noteworthy that most phenyl nanocarbons derived from porphyrin have been found to lack complete  $\pi$ -conjugation. The introduction of  $\beta,\beta'$ -doubly 2,6-pyridylene blocks resulted in unusually bent conformations, presenting a challenge until the successful development of the Ni(II)-porphyrin cage [90]. The tubular cage, **COC-12**, was synthesized via a quadruple Suzuki-Miyaura cross-coupling reaction of compounds **18** and **19** (Fig. 9). Analysis using SC-XRD reveals that the pyridine groups are tilted at an angle of  $43.5^\circ$  relative to the neighboring pyrrole units. This configuration enables the pyridine to act as a mediator, facilitating moderate overall  $\pi$ -conjugation. Moreover, a  $\text{C}_{60}$  molecule was successfully encapsulated within the cavity of **COC-12**, which has an average diameter of approximately  $3.6 \text{ \AA}$ . This successful encapsulation can be attributed not only to favorable structural features—such as optimal pyrrole-pyridine distances ( $1.45\text{--}1.50 \text{ \AA}$ ), dihedral angles between pyridines and porphyrins ( $50\text{--}53^\circ$ ), and spacious voids ( $14 \text{ \AA}$  in diameter)—but also to cooperative interactions between the  $\text{C}_{60}$  molecule and the concave wall formed by the ruffled porphyrins. This is further supported by evidence from UV-vis absorption spectra and  $^{13}\text{C}$  NMR spectroscopy analyses.

## 3. cCOCs bridged by double bond

cCOCs connected by  $\text{C}=\text{C}$  or  $\text{C}=\text{N}$  bonds are referred to as cCOCs bridged by double bond. The inception of this field can be traced back to the discovery of bicyclophanehexaene with a cage-like structure in 1977 [52]. However, significant interest in this area resurged in 2018,

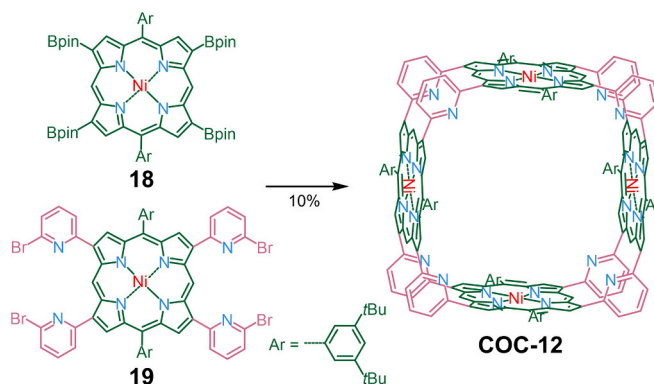


Fig. 9. Tubular COC-12 synthesized via the quadruple Suzuki-Miyaura cross-coupling reaction.

particularly regarding the synthesis of fully conjugated 3D carboporphyrin cages [46]. Recently, the use of porphyrin analogues and thiophene units as key components has gained popularity in constructing highly distorted 3D cages. These components enhance coupling pathways within the conjugated system and promote electron delocalization more effectively than conventional benzene rings [27,28,45,58]. Consequently, preliminary investigations into how the symmetry of cCOCs influences their  $\pi$ -conjugated pathways have made notable strides, fueled by rapid advancements in various types of double bond-based cCOCs. These findings lay a crucial foundation for future explorations into 3D aromaticity. cCOCs bridged through C=C or C=N bonds can be effectively synthesized using advanced strategies, including the Wittig reaction, Knoevenagel reaction, olefin metathesis, Perkin reaction, resonance aromatization (involving phenylmethene, thiophenemethene, and pyrromethene), Schiff base reactions, and so on (Fig. 10).

### 3.1. Ethylene bridged cCOCs

Taking into account the stability of ylids and the reactivity of aldehydes, Hans-Erik Högberg chose **20** and **21** as reactants to minimize their spatial interactions, facilitating the one-step synthesis of bicyclopentane via a Wittig reaction [52]. The resulting caged bicyclopentane, **COC-13**, displays high symmetry along with a certain degree of flexibility (Fig. 11). This is further substantiated by the  $^1\text{H}$  NMR spectra, which reveals signals corresponding to only four distinct sets of protons, as well as the presence of a singlet state for the protons located in the *para*-substituted ring. This development marks a significant milestone in the synthesis of cage-type compounds, representing the first successful synthesis of cCOC structures.

In 2018, Prof. Sessler successfully synthesized the largest 3D carboporphyrin cage, **COC-14**. This remarkable structure is composed of four dipyrromethene units and two dibenzo[*g,p*]chrysene units, synthesized through a one-pot condensation reaction followed by oxidation (Fig. 12A) [46]. The two dibenzo[*g,p*]chrysene fragments are arranged in a face-to-face orientation, with an approximate distance of 8.522 Å between the midpoints of the central C—C bonds of each chrysene subunit. Additionally, these fragments exhibit a dihedral angle of 59.9°

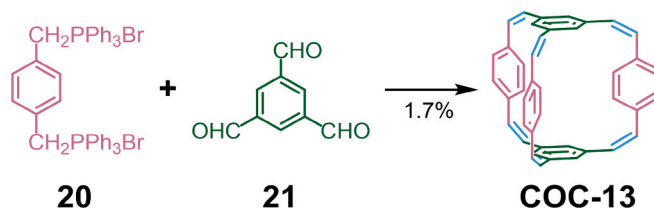


Fig. 11. Wittig reaction to construct **COC-13**.

between their outer benzene planes, indicating a notable degree of distortion in the dibenzo[*g,p*]chrysene bridge. It is particularly noteworthy that the dimensions and electronic properties of **COC-14** can be modulated through protonation. The nucleus-independent chemical shift (NICS) value of the neutral cage is nearly zero (−1.75), suggesting its non-aromatic character. However, upon protonation with trifluoroacetic acid (TFA), **COC-14** transitions to a globally aromatic form, as indicated by a significantly altered NICS value of −11.63. Furthermore, due to the presence of the inner mesityl groups, the limited cavity of the neutral cage can be expanded during protonation, resulting in the release of these groups, as revealed by SC-XRD analyses. In 2022, Prof. Kim reported an additional instance of a conjugated carboporphyrin cage, synthesized from a rigidly substituted pyrene precursor [27]. This precursor (**23**) underwent a [6 + 3] condensation reaction with pentafluorobenzaldehyde, yielding two isomers, **COC-15A** and **COC-15B** (Fig. 12B). Both isomers possess diameters exceeding 1 nm and are composed of three bridging pyrene units along with six dipyrromethene moieties. Specifically, **COC-15A** features one transversely oriented and two vertically oriented pyrene units, whereas all three pyrene units in **COC-15B** are vertically oriented. This arrangement leads to significant distortion in **COC-15B**, which exhibits larger dihedral angles (13.7°, 14.8°, and 21.3°) and greater intrinsic strain compared to **COC-15A** (13.3°, 16.0°, and 2.4°). Furthermore, this unique property of **COC-15B** is leveraged to synthesize an unprecedented zinc complex, which includes seven interconnected Zn<sup>2+</sup> cations bridged by oxygen atoms and coordinated with the dipyrromethene subunits, as confirmed by SC-XRD analysis. Notably, unlike previously reported porphyrin systems that relied on pre-metallized precursors, this condensation strategy may pave the way for the development of heteroatomic cages and their metal complexes, significantly advancing the potential for creating larger conjugated systems with promising future applications.

In order to further investigate the fundamental aromatic principles of

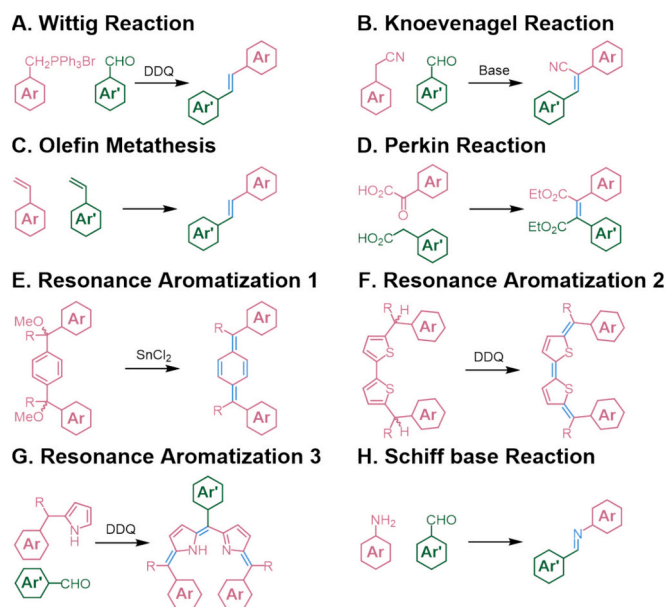


Fig. 10. Synthetic approaches for cCOCs bridged by double bond. (A) Wittig reaction; (B) Knoevenagel reaction; (C) olefin metathesis; (D) Perkin reaction; (E–G) Resonance aromatization of phenylmethene, thiophenemethene, and pyrromethene; (H) Schiff base reaction.

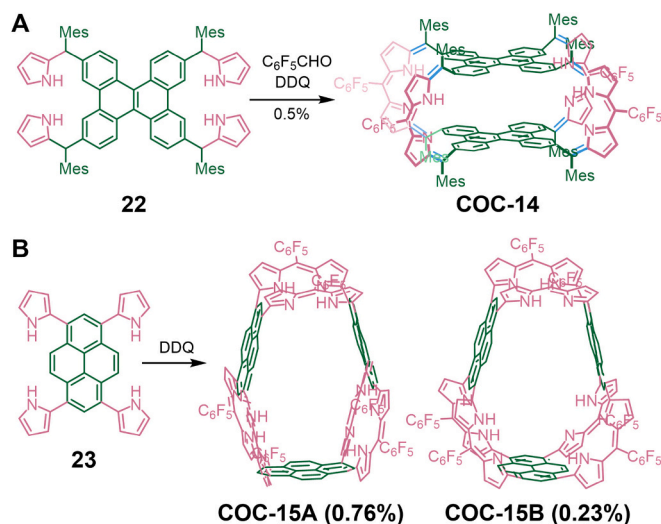


Fig. 12. The resonance aromatization of dipyrromethene-based cCOCs, **COC-14** and **COC-15**, through the condensation of arylaldehyde and pyrrole followed oxidation.

3D cCOCs, Prof. Wu designed a four-fold symmetric cage, **COC-16**, which incorporates two porphyrin moieties and four thiophene-based arms [28]. The synthesis involved an intermolecular Yamamoto coupling reaction, followed by oxidative dehydrogenation of the isolated octahydro-cage (**25**) to yield **COC-16** (Fig. 13A). X-ray crystallographic analysis reveals that the structure of **COC-16** resembles an inclined cage featuring a  $C_2$  symmetric center. This cage includes two nearly planar and parallel porphyrin rings that are spaced approximately 7.8 Å apart. Interestingly, when subjected to two-electron oxidation, **COC-16** transforms into **COC-16**<sup>2+</sup> as a 3D globally aromatic species. This transformation allows all five forms of the associated two-dimensional (2D) macrocycles to exhibit Hückel aromaticity. In contrast, the neutral **COC-16** itself only demonstrates local aromaticity confined to its porphyrin units. The observed 3D electron delocalization in **COC-16**<sup>2+</sup> is attributed to the specific arrangement of the porphyrin [91–93] and thiophene rings [94,95], which facilitates effective overlap of  $\pi$  orbitals. Notably, X-ray crystal analysis indicates that **COC-16**<sup>2+</sup> experiences smaller distortion angles between the porphyrins and adjacent thiophene units when compared to neutral **COC-16**. This reduction in distortion angles signifies enhanced  $\pi$  orbital overlap, indicative of a more stable and planar arrangement. Furthermore, the distance between the two porphyrin units increases, averaging approximately 10.3 Å, suggesting that oxidation plays a crucial role in inducing significant structural changes. This oxidation not only alleviates strain within the cage structure but also promotes the delocalization of  $\pi$  electrons throughout the 3D skeleton. In summary, the oxidation procession represents a key transformation that enhances aromatic properties through increased electron delocalization and structural optimization.

In the context of **COC-16**, it has been demonstrated that the presence of bridged porphyrinoids alone is insufficient to ensure 3D aromaticity, as the electron delocalization predominantly occurs within just one of the macrocycles [46,96–98]. To address this, Wu's group developed a symmetrical polyradicaloid cage featuring three identical conjugated bridges interconnecting two carbon-centered radicals [45]. The connectivity of the radicals through any of the bridges can lead to a closed-shell configuration characterized by reduced symmetry due to antiferromagnetic coupling. The researchers synthesized a dimeric cage precursor (**27**) via Yamamoto homocoupling, followed by oxidative dehydrogenation using DDQ, resulting in the formation of a fully  $\pi$ -conjugated cage, **COC-17** (Fig. 13B). Subsequently, Prof. Wu and Kim conducted an investigation into the aromaticity associated with various oxidation states of **COC-17**. Their findings revealed that the neutral cage exhibits an open-shell singlet ground state, predominantly comprising

38  $\pi$ -electrons, in alignment with the  $[4n + 2]$  Hückel aromatic rule. Moreover, **COC-17** has the ability to undergo chemical oxidation to produce multiple cationic states in a controlled fashion by utilizing different amounts of the oxidizing agent  $\text{NO}\cdot\text{SbF}_6$ . Notably, the **COC-17**<sup>2+</sup> state manifests a triplet ground state with 36  $\pi$ -electrons, thereby satisfying the criteria laid out by the  $[4n]$  Baird aromatic rule [99]. In contrast, the **COC-17**<sup>4+</sup> species exists as an open-shell singlet with 52  $\pi$ -electrons distributed throughout its rigid structure, showcasing traits of 3D global antiaromaticity. Lastly, the **COC-17**<sup>6+</sup> model displays  $D_3$  symmetry, exhibiting  $[6n + 2]$  3D global aromaticity due to the even distribution of its 50  $\pi$ -electrons [47]. The exploration of these 3D  $\pi$ -conjugated systems reveals that they strive to reach their lowest energy configurations by modifying their geometry, spin states, and associated aromatic properties. Additionally, Prof. Wu also successfully synthesized highly symmetrical radical cCOCs utilizing the classical Yamamoto coupling reaction, which correlates with two studies conducted in 2020 [29,45]. Through this research, they were able to evaluate the electronic characteristics and aromatic nature of various oxidation states, compellingly demonstrating that the concept of 3D global aromaticity can indeed be explained in terms of the 2D Hückel aromaticity of individual aromatic macrocycles within the overarching 3D  $\pi$ -conjugated skeleton. This discovery further solidifies a universal principle:  $\pi$ -conjugated molecules inherently tend to adopt an aromatic configuration, as such structures represent the most energetically favorable states [28].

Numerous ongoing efforts to synthesize novel radical cCOCs have continued without interruption. Anand has sought to streamline the synthesis of appropriate precursors for a potential isophlorinoid dimer, leading to a fortuitous discovery of a fully conjugated tetrapod cage structure, **COC-18**, which consists of sixteen thiophene units (Fig. 13C) [58,100]. The synthesis of **COC-18** involves the combination of tetra-thienylethene (**28**) and bithiophene diol (**29**) in a precise ratio, facilitated by the catalysis of boron trifluoride etherate, followed by oxidation with DDQ. Notably, **COC-18** displays  $C_4$  symmetry, with all sulfur atoms oriented towards its center. The bridgeheads of the two tetra-thienylethene units are separated by a distance of 9.21 Å, while the *meso* carbon atoms positioned diagonally opposite each other are spaced 13.11 Å apart. The pre-designed precursors containing thiophene moieties introduce reactive steric hindrance, which significantly favors the formation of 3D cage structures and quasi-cage compounds over macrocycles. However, a notable challenge lies in the reduced production yield and the tendency for undesired macrocyclic formations, influenced by the steric hindrance associated with the heterocyclic precursors.

To enhance the understanding of the influence of structural rigidity

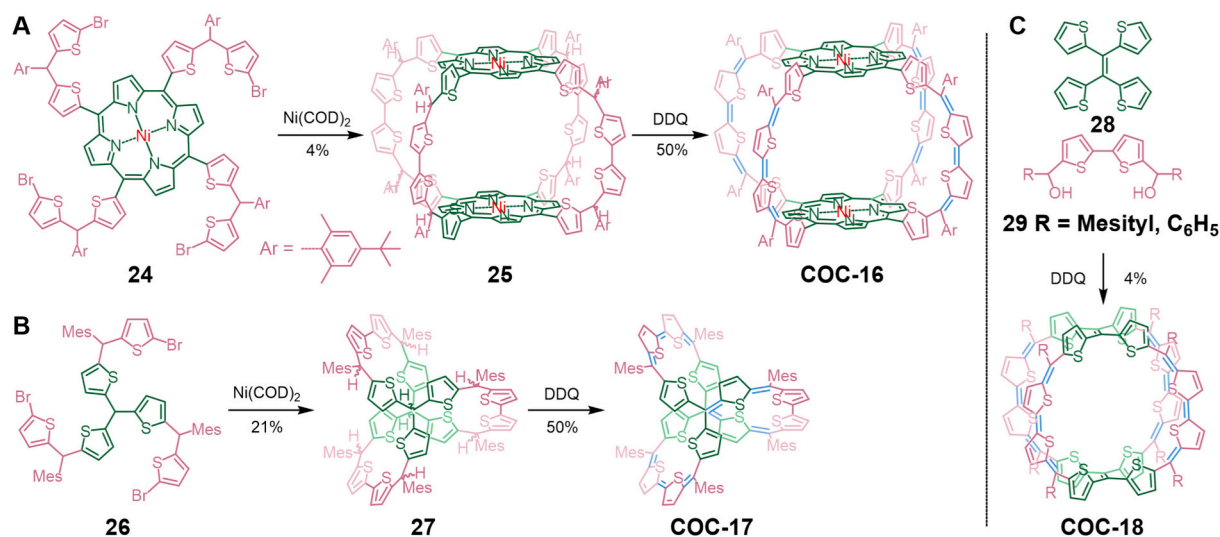


Fig. 13. Resonance aromatization of bithiophene based cCOCs, **COC-16** ~ **COC-18**.

on the dynamics, stability, and electronic characteristics of diradicaloids and polyradicaloids, Prof. Wu successfully synthesized a 3D polyradicaloid cage, **COC-19**, which is composed of three Chichibabin's hydrocarbon (CH) motifs linked by two benzene-1,3,5-triyl moieties [29]. The synthesis process experiences challenges due to steric hindrance caused by the bulky mesityl groups interacting with adjacent phenyl moieties in the precursor compounds (**30**). This results in an optimal dihedral angle that facilitates the Yamamoto homocoupling reaction, ultimately leading to a 26 % yield of the cage precursors (**31**). Subsequent to this, a six-fold reductive elimination of the methoxy groups in the caged precursors using  $\text{SnCl}_2$  yielded **COC-19** with nearly quantitative efficiency (Fig. 14A). The individual CH units within **COC-19** exhibit a propensity to form open-shell diradicals, which is anticipated to be a key contributor to the compound's diradical properties. The presence of bulky mesityl groups not only provides structural congestion but also imparts kinetic stabilization—ensuring that all CH units adopt a *cis*-configuration [101]. Consequently, **COC-19** displays enhanced stability, a reduced diradical character, and an increased singlet-triplet energy gap, attributed to higher rotational energy barriers associated with its quinoidal biphenyl units. Moreover, the ellipsoidal cavity of **COC-19** is adeptly sized to accommodate a  $\text{C}_{70}$  molecule, indicating a clear preference for  $\text{C}_{70}$  over  $\text{C}_{60}$ . Additionally, **COC-19** can be oxidized into various cationic states when exposed to corresponding equivalents of  $\text{NO}\cdot\text{SbF}_6$ . The presence of aromatic biphenyl subunits in the oxidized form, **COC-19**<sup>9+</sup>, is confirmed through X-ray crystallography, supported by UV-vis absorption and Raman spectroscopy analyses. In its crystalline form, **COC-19**<sup>6+</sup> exhibits a distinct one-dimensional columnar structure, achieved through intermolecular  $\pi$ - $\pi$  stacking of the benzene-1,3,5-triyl bridgeheads.

The research conducted by Prof. Chi demonstrates a sophisticated approach to synthesizing novel conjugated cages, **COC-20-TPA** and **COC-20-Cz**, through the oxidative dehydrogenation of non-conjugated 1,3,5-tribenzene bridged cage precursors (**32** and **33**) (Fig. 14B) [102]. The three-armed **COC-20-TPA** is noted for its flexible structure, while **COC-20-Cz** displays a more rigid architecture, confirmed by NMR and X-ray crystallography analysis. The variable temperature NMR measurements of **COC-20-TPA** reveal its unique thermally responsive intramolecular dynamics, particularly the movement of the phenyl rings within the structure. Interestingly, the photoluminescence quantum yield of **COC-20-TPA** in solid-state conditions is significantly higher (4.8 % at 626 nm) compared to its yield in solution (1.2 % at 600 nm), highlighting its aggregation-induced emission (AIE) behaviors. On the other hand, **COC-20-Cz** does not exhibit AIE characteristics, which can

be attributed to the rigidity of its carbazole subunits. The findings underline the potential of **COC-20-TPA** as a new class of quinoidal AIE agents, thereby reaffirming the effectiveness of the resonance aromatization strategy in the development of 2D or 3D conjugated materials endowed with novel optoelectronic properties.

In a recent study conducted by Prof. Yuan in 2023, a one-step Knoevenagel reaction catalyzed by a base was employed to synthesize  $sp^2$  cCOCs [42]. Various aromatic diacetonitriles, including **35a**, **35b**, **35c**, and **35d**, were utilized as linking agents to effectively connect different bowl-shaped aromatic trialdehydes (**34a** and **34b**), via a [2 + 3] condensation reaction (Fig. 15). This approach results in the high-efficiency synthesis of a series of  $sp^2$  cCOCs characterized by similar triangular prism structures but with varying external substituents. As a notable example, **COC-21**, synthesized from **34b** and **35b**, possesses a monoclinic crystal structure with a space group of *P*-21c through SC-XRD analysis. This compound features a twisted triangular prism with a height of 1.15 nm. The intrinsic void diameter and the average diameter of the cage's circular window are measured to be approximately 5.6 Å and 4.8 Å, respectively, leading to a calculated volume of 222 Å<sup>3</sup> within the cage structure. Further analysis of the crystal voids in **COC-21** is performed using Mercury software alongside a nitrogen probe with a kinetic radius of 1.82 Å, which indicates that 22 % of the unit cell volume is capable of accommodating gas molecules. **COC-21** demonstrates a strong adsorption capacity for various gases, including  $\text{CO}_2$ ,  $\text{CH}_4$ , and  $\text{C}_2$  hydrocarbons, and exhibits effective separation capabilities for  $\text{CO}_2/\text{N}_2$  and  $\text{CO}_2/\text{CH}_4$  gas mixtures. Additionally, extensive studies focusing on the chemical and thermal stability of the synthesized cCOCs underscore their exceptional stability. Notably, these structures maintain their structural integrity when exposed to aggressive environments, including concentrated HCl, concentrated  $\text{HNO}_3$ , and saturated NaOH solutions.

### 3.2. Imine bridged cCOCs

In conventional understanding, the dynamic reversibility of imine bonds results in imine-linked cCOCs being less stable than those linked by irreversible covalent bonds. This instability stems from the susceptibility of imine bonds to hydrolysis under various conditions, including acidic, alkaline, and even aqueous environments, which significantly limits their potential applications [103–111]. To address this challenge, many researchers have adopted post-synthesis modification (PSM) strategies to transform imine bonds into more robust linkages such as imide [112], quinoline [113], carbamate [114], or carbon-carbon bonds

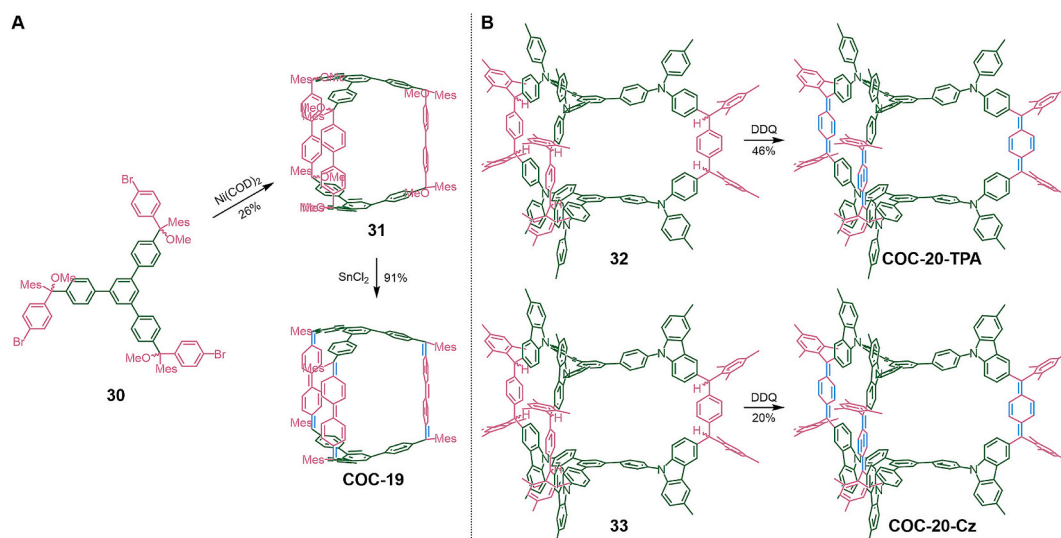


Fig. 14. Resonance aromatization of biphenyl-based cCOCs, **COC-19** and **COC-20**.

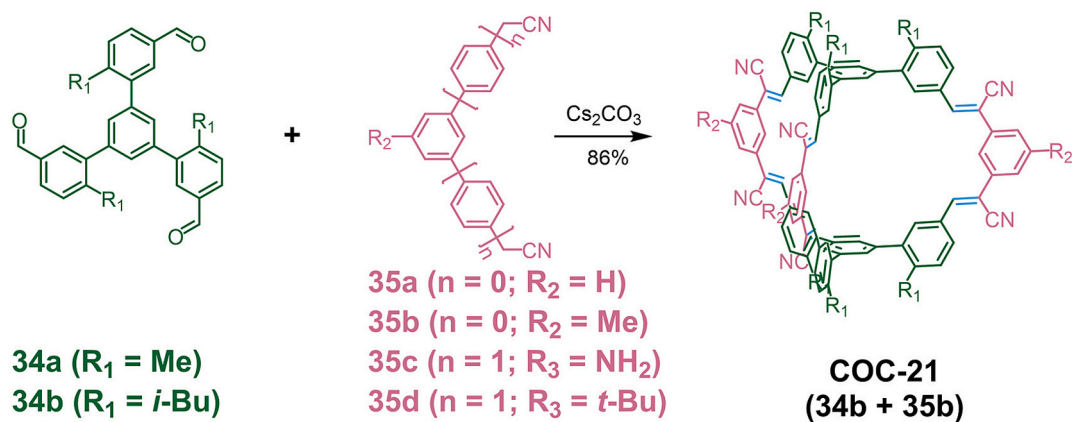


Fig. 15. Synthesis of olefin COC-21 through Knoevenagel reaction.

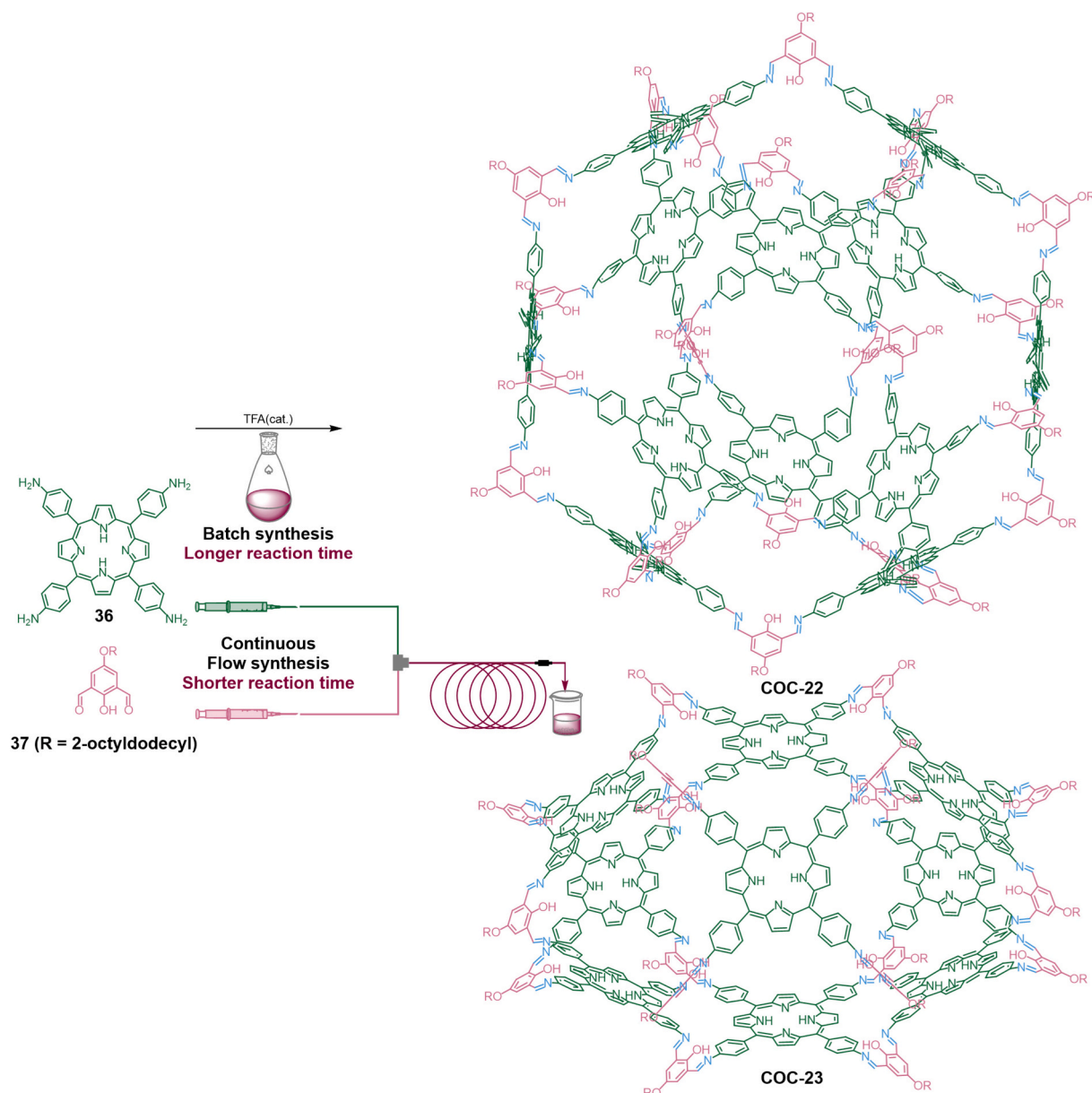


Fig. 16. Giant porphyrin cages, COC-22 and COC-23, through dynamic Schiff base reaction.

[115]. Despite the inherent instability of imine bonds, their dynamic nature can actually confer some advantageous properties, such as allowing for “error-checking” and “proofreading” processes. This capability enables the formation of the most thermodynamically stable assemblies due to the reversible nature [116–120]. The careful selection of appropriate aryl building blocks for imine condensation plays a crucial role in facilitating the synthesis of cCOCs with high yields. This approach not only simplifies the synthesis process—avoiding the complexities typically associated with multi-step organic methods—but also helps reduce the generation of polymer by-products. Several noteworthy studies have explored the realm of imine-linked cCOCs, highlighting their potential and offering insights into optimizing their stability and functionality.

Leveraging the dynamic nature of the imine bond allows for the construction of large cages that can effectively impress undesired polymer by-products and facilitate the formation of a limited number of larger cages, as opposed to a multitude of smaller ones. In their noteworthy work, Prof. Kim introduced a Schiff base reaction designated as  $[2n + 4n]$ , utilizing square porphyrin derivatives (P) in conjunction with curved two-connecting linkers (L) to create a series of substantial porphyrin cages [37,38]. One such substantial structure, the giant porphyrin cage, **COC-22**, is synthesized with the chemical formula  $P_{12}L_{24}$ , which combines twelve **36** as the scaffold and twenty-four **37** as linkers (Fig. 16) [37]. The assembled **COC-22** features an outer diameter of approximately 5.3 nm coupled with an internal void space of around 4.3 nm. Within its crystalline architecture, the cages are arranged in a face-centered and densely packed configuration, which leads to the emergence of tetrahedral and octahedral extrinsic voids with diameters of 1.6 nm and 2.2 nm, respectively. Interactions between alkyl chains and salicylic moieties from adjacent cages occur via weak hydrogen bonding (specifically C—H $\cdots\pi$  interactions), along with somewhat offset porphyrin-porphyrin stacking observed at a distance of 3.7 Å. Due to its hollow architecture and absence of metal atoms, **COC-22** is characterized by an exceptionally low density (approximately 0.29 g/cm<sup>3</sup>) and a remarkably high solvent-accessible volume (around 75.4 %), within the realm of molecular crystals. The heterogeneous photocatalytic performance of **COC-22** underscores the importance of its expansive internal cavity and channel, which significantly enhances the transport of larger substrates and products during catalytic reactions. Particularly noteworthy is the photocatalytic oxidation rate for larger substrates, such as dihydroxynaphthalene derivatives, which is found to be substantially higher in **COC-22** compared to its smaller porphyrin counterparts. Moreover, following the metallization of **COC-22** with zinc, a pyridine-capped fitting is introduced that may partially engage with the Zn(II) porphyrin entities located at opposite faces within **Zn-COC-22**, effectively spanning the internal cavity. This demonstration of guest encapsulation provides compelling evidence for the potential to streamline the synthesis of large cages endowed with specific functionalities within their extensive voids—an endeavor that is often challenging when attempting to position functional groups in close proximity.

The dynamic formation of forty-eight reversible imine bonds during the self-assembly of **COC-22** necessitates a lengthy error correction process, often requiring high dilution conditions and extended reaction times of 3–5 days [37]. In contrast, flow chemistry can efficiently transfer mass and heat under continuous flow conditions, facilitating the self-assembly of reactants [121]. This approach enables large-scale synthesis of cage products in a significantly shorter timeframe, addressing the challenges associated with traditional batch synthesis in laboratory settings [122]. To enhance the protective encapsulation of functional guest macromolecules, Prof. Kim focused on developing a continuous flow process to optimize the synthesis of **COC-22** and to discover **COC-23**, characterized by the formula  $P_9L_{18}$  as a new kinetic product. Compared to the previously reported batch synthesis of **COC-22**, which yields approximately 38 % with a reaction time of 3 to 5 days, the optimized continuous flow method achieves a yield of 65 % within a residence time of just 110 min at 120 °C. Additionally, PM3 model

calculations indicate that the newly formed **COC-23** exhibits a triangular prism geometry, with ellipsoidal dimensions of 3.2 nm along the minor axis and 4.2 nm along the major axis. This cage demonstrates  $D_{3h}$  point symmetry, comprising two groups of porphyrins: six porphyrins that form the vertices of the trigonal prism and three porphyrins that serve as tricapped vertices. While the flow synthesis does not allow for the isolation of this cage, its emergence underscores that continuous flow processes provide an alternative pathway for the self-assembly of molecular cages with diverse topologies under non-equilibrium conditions.

In addition to the construction of large cages, Schiff base reactions are also utilized in the synthesis of cage catenanes [43,44]. The building blocks *m*-terphenyl diamine and trialdehyde 1,3,5-triformylbenzene (**41**) can facilitate  $[6 + 4]$  condensation with TFA as catalyst, leading to the formation of cage catenane, **COC-24**, interlocked by two symmetrical imine cages (Fig. 17) [43]. The enhanced hydrolytic stability of **COC-24** compared to a single cage is likely attributed to the efficient  $\pi$ - $\pi$  stacking between the parallel-oriented aryl sheets. The presence of these sheets within the void of the partner cage acts as a stabilizing template, ensuring the structural integrity of the entire interlocked scaffold. Furthermore, **COC-24** can be transformed into a catenane (**38**) with dissymmetric cages that possess only a  $C_3$ -symmetric axis. This transformation is achieved through the selective reduction of the outer imine plates using the bulky reductant sodium triacetoxyborohydride (NaBH(OAc)<sub>3</sub>), which is facilitated by the limited spatial volume of the interlocked inner cavity. This synthetic strategy enables the development of advanced topologies for catenated cages, paving the way for the discovery of new functional materials, including D-A-D'-A' catenanes, interlocked cages, and poly(interlocked cages), which are promising for applications in ferroelectrics, light-emitting materials, and more.

In 2022, Prof. Zhao serendipitously synthesized an interlocked cage, **COC-25**, through a Schiff base reaction involving the precursors **39** and **40** (Fig. 18) [44]. SC-XRD analysis clearly reveals the self-assembly of triangular prism cage catenanes in a “head-to-tail” configuration along the *b*-axis, resulting in the formation of a 2D layer in the *bc* plane. The creation of this catenane structure is driven by several factors, notably the significant influence of  $\pi$ - $\pi$  interactions during the assembly process. These interactions extend beyond the connections between anthracene and triphenylbenzene units to include interactions between the anthracene molecules themselves. The triphenylbenzene units located within the partner cage's cavity act in a preassembled manner prior to being encapsulated during the processes of preorganization and self-repair. Additionally, there is interpenetration among the cages, leading to the formation of a void structure. The careful selection of appropriate structures and sizes is crucial, as illustrated by the replacement of the central moiety from triphenylbenzene with benzene or triphenylamine. This alteration results in the formation of only two monomeric cages, **COC-26** and **COC-27**.

Prof. Cooper also employed reactants **39** and **41** as precursors to synthesize conjugated imine cages, **COC-26**, for investigating host-guest complexation and fabricating co-crystal materials [50]. These cages assembled into a porous host with two distinct extrinsic voids, from which a series of co-crystals were engineered. Packing coefficients (PCs) are utilized to assess the feasibility of encapsulating the guest by calculating the body cavity and guest volume, ensuring that the maximum dimensions were not exceeded. Specifically, a host-imine cage forms a co-crystal solid with five organic guests of similar size, resulting in an isoskeletal structure. The co-crystals are designed using cost-effective computational techniques to identify suitable components, achieving a PC ranging from 44 % to 50 %, while also considering the shape of the guest molecules. Furthermore, by incorporating the high-emission BODIPY guest into the host structure, the photoluminescence properties associated with its two-photon excitation can be amplified by a factor of six. This demonstrates that the co-crystal design approach can also be extended to challenging ternary organic crystals, which can be achieved by introducing specific guests into voids

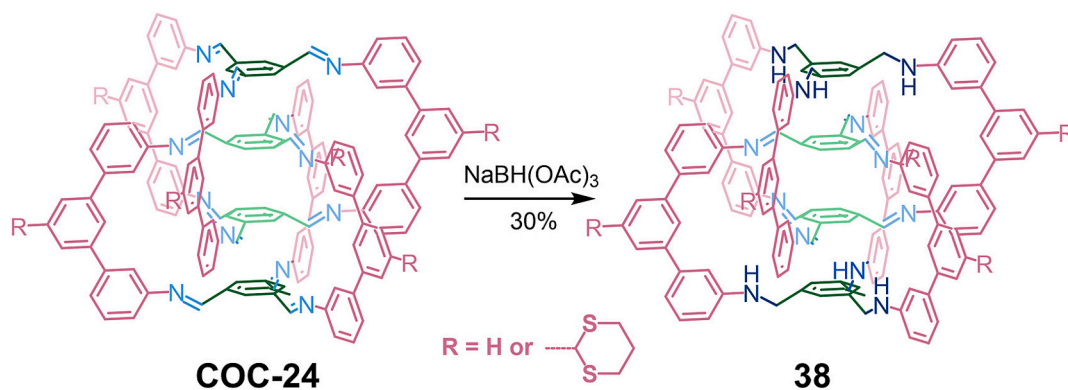


Fig. 17. cCOC catenane, COC-24, and its asymmetrically reduced cage catenane.

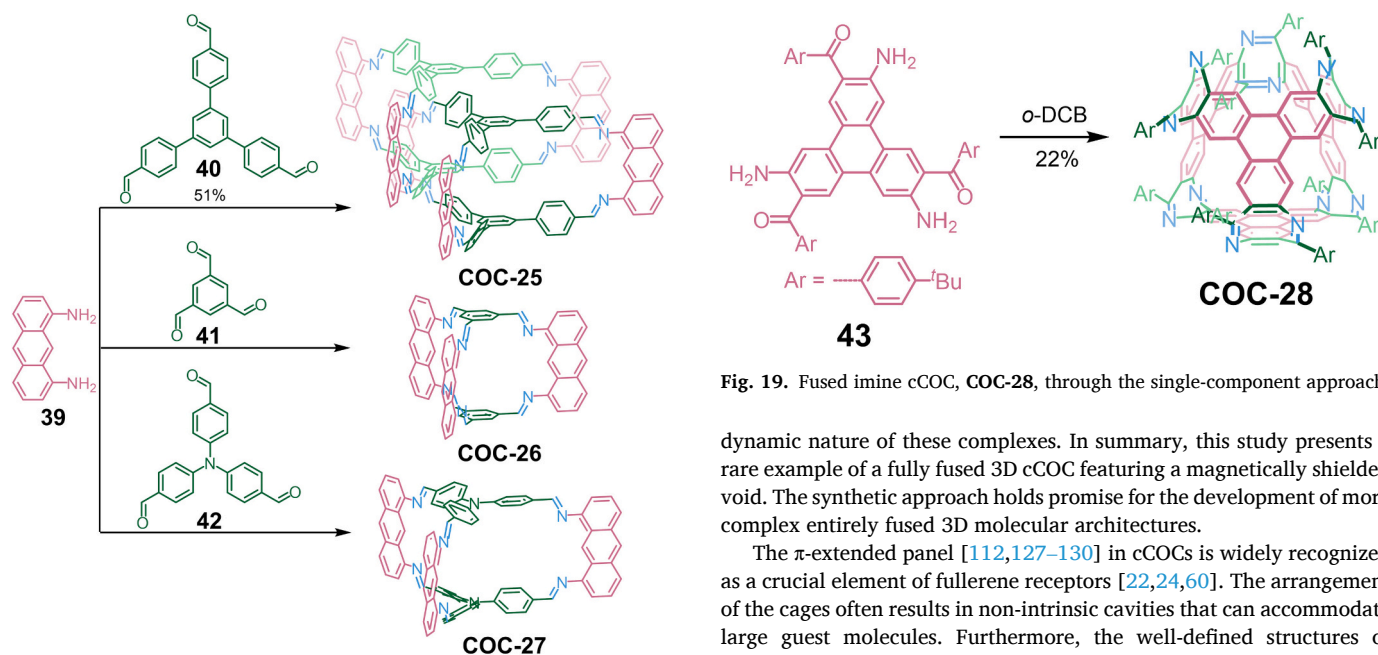


Fig. 18. Imine based COC-25–27 with different capped moieties.

of varying sizes within the host.

In 2021, Prof. Wu successfully synthesized a fully conjugated imine cage, **COC-28**, which demonstrates superior stability compared to other imine-linked cages [123]. A crucial feedstock, *tris*-2-amino-benzophenone (**43**) [124], can undergo self-condensation to form a truncated tetrahedral cage through acid-catalysis in *o*-dichlorobenzene (*o*-DCB) (Fig. 19). This solvent not only serves as a reaction medium but also acts as a template that facilitates cage closure. Unlike conventional imine cages, **COC-28**, based on [1,5]diazocine, exhibits remarkable stability, remaining intact under harsh conditions such as exposure to 1 M HCl or KOH. The high symmetry of *o*-DCB/COC-28 is reflected in its single crystals, which exhibit both triangular and hexagonal facets. Short contact analysis reveals a range of intermolecular interactions between **COC-28** and *o*-DCB, forming host-guest complexes characterized by  $\pi \cdots \pi$ , C–H $\cdots\pi$ , and halogen $\cdots\pi$  interactions. The mean dihedral angle of the eight-membered ring is found to be approximately 73°, aligning with the typical values observed in structures containing [1,5]diazocines (approximately 72–75°). This finding indicates that the intrinsic curvature of [1,5]diazocines imposes minimal strain, making them particularly well-suited for such structural designs [125,126]. Furthermore, investigations into host-guest chemistry reveal that *o*-DCB can be partially displaced by competing molecules, underscoring the

Fig. 19. Fused imine cCOC, COC-28, through the single-component approach.

dynamic nature of these complexes. In summary, this study presents a rare example of a fully fused 3D cCOC featuring a magnetically shielded void. The synthetic approach holds promise for the development of more complex entirely fused 3D molecular architectures.

The  $\pi$ -extended panel [112,127–130] in cCOCs is widely recognized as a crucial element of fullerene receptors [22,24,60]. The arrangement of the cages often results in non-intrinsic cavities that can accommodate large guest molecules. Furthermore, the well-defined structures of cCOCs enable detailed investigations into host-guest interactions [30,50,51]. Recently, Prof. Sun proposed the initial instance of a crystalline axially chiral cCOCs based on imine with excellent stability derived from chiral *R/S*-**45a** or *R/S*-**45b** and **44** (Fig. 20) [51]. SC-XRD analysis demonstrates that enantiopure **COC-29A** and **COC-29B** (e.g., *R* configuration) are isostructural, crystallizing in the cubic *I*4<sub>1</sub>32 space group. **COC-29A** exhibits a capsule-like appearance, with two planes linked by three “paddle” structures from the binaphthyl moiety. Although both *R*-**COC-29A** and *R*-**COC-29B** single capsules are formally

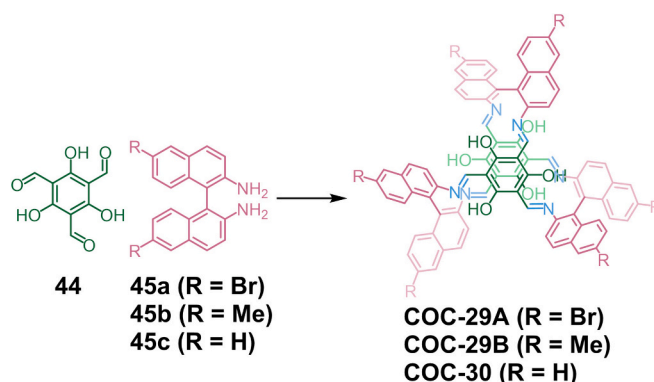


Fig. 20. Synthesis of chiral imine cCOCs, COC-29 and COC-30.

non-porous, they feature distinct lattice voids. These capsule-shaped cCOCs are arranged in a 3D supramolecular structure through  $\pi$ - $\pi$  interactions, resulting in pore sizes of  $24.88 \times 24.88$  and  $24.84 \times 24.84 \text{ \AA}^2$  for **R-COC-29A** and **R-COC-29B**, respectively. The estimated internal void volumes are approximately 24,508 and 24,335  $\text{\AA}^3$ . Moreover, the adsorption isotherms at 77 K exhibit type I behavior, indicating narrow pore widths of 23.4 and 21.6  $\text{\AA}$  for **R-COC-29A** and **R-COC-29B**. Given the accessible and spacious cavities, the capability of these cages to encapsulate fullerenes is investigated. In situ encapsulation experiments with  $C_{60}$  and  $C_{70}$  result in dark crystalline samples within enantiopure **COC-29A**. Notably,  $C_{70}$  can be selectively extracted from fullerene carbon soot, demonstrating a  $C_{70}/C_{60}$  ratio of 5–50 % for **COC-29A**, while **COC-29B** shows no uptake of fullerenes under identical conditions. The preference for  $C_{70}$  is largely attributed to electrostatic interactions between the arene and fullerene, as well as the influence of electron-withdrawing substituents, as supported by both experimental data and density functional theory (DFT) calculations. In addition to encapsulation, the transfer of chiroptical features from **R-COC-29A** and **S-COC-29A** to  $C_{60}$  and  $C_{70}$  is observed, corroborated by SC-XRD analysis and intense circular dichroism signals. In summary, the cCOC-fullerene complexes not only perturb the inherent symmetrical electronic configuration of fullerenes but also induce their chiroptical features. This research expands the scope of chiral porous aromatic cCOCs and provides novel insights into the separation of fullerenes from sooty carbon and the induction of chirality in these molecules.

The same research group has also successfully synthesized a hierarchically porous  $\pi$ -stacked organic framework (Cage- $\pi$ OF) featuring spring-like behavior based on chiral cage, **COC-30**, using **44** and **R/S-45c** as raw materials. The study also explored the photoluminescence color-changing behavior of Cage- $\pi$ OF under ultra-high pressure conditions [30]. SC-XRD analysis reveals that the **COC-30** enantiomer

crystallizes in the chiral space groups  $P4_132$  (for the *R* configuration) and  $P4_332$  (for the *S* configuration), with a centroid distance of 3.869  $\text{\AA}$  between neighboring binaphthyl rings. Each **COC-30** unit connects to three neighboring cages via intermolecular interactions among the benzene rings present within three binaphthyl fragments, thereby forming a 3D porous supramolecular structure. The  $\pi$ - $\pi$  interactions among the molecular cages play a crucial role in regulating structural shrinkage. Additionally, the elasticity provided by the porous spring structure significantly contributes to the material's outstanding compression-induced fluorescence discoloration. With a bulk modulus of 9.5 GPa, Cage- $\pi$ OF exhibits softer elastic properties compared to most crystalline porous materials (CPMs) reported in literature. Notably, its collapse point at 20.0 GPa exceeds that of previously documented CPMs. Cage- $\pi$ OF demonstrates superior performance in piezofluorochromism, exhibiting a linear pressure-responsive shift in emitted color and a significant emission difference of 154 nm (shifting from 547 nm to 701 nm) with a maximum response at 16 GPa. This advancement broadens the landscape of smart luminescent materials.

The utilization of molecular cages in the realm of controlled host-guest chemistry has garnered significant attention [39,40,117,123]. In particular, the development of molecular cages with gated molecular recognition holds great potential for advancing applications in membranes, drug delivery systems, and catalysts [39,40]. In 2014, Prof. Nabeshima designed a novel type of helical imine cage, **COC-31A**, capable of forming cryptand-like metallocryptands with three nickel(II) ions. The presence of six phenoxo groups for coordination and two pivotal benzene rings for  $\pi$ -stacking allows this trinickel(II) metallocryptand to form a stable inclusion complex with guanidinium ions [39,131,132]. Building upon this foundation, they introduced an innovative metallo cage that can close its aperture via coordination (Fig. 21) [40]. After coordinating with cobalt(III) ions, the saloph tetradentate

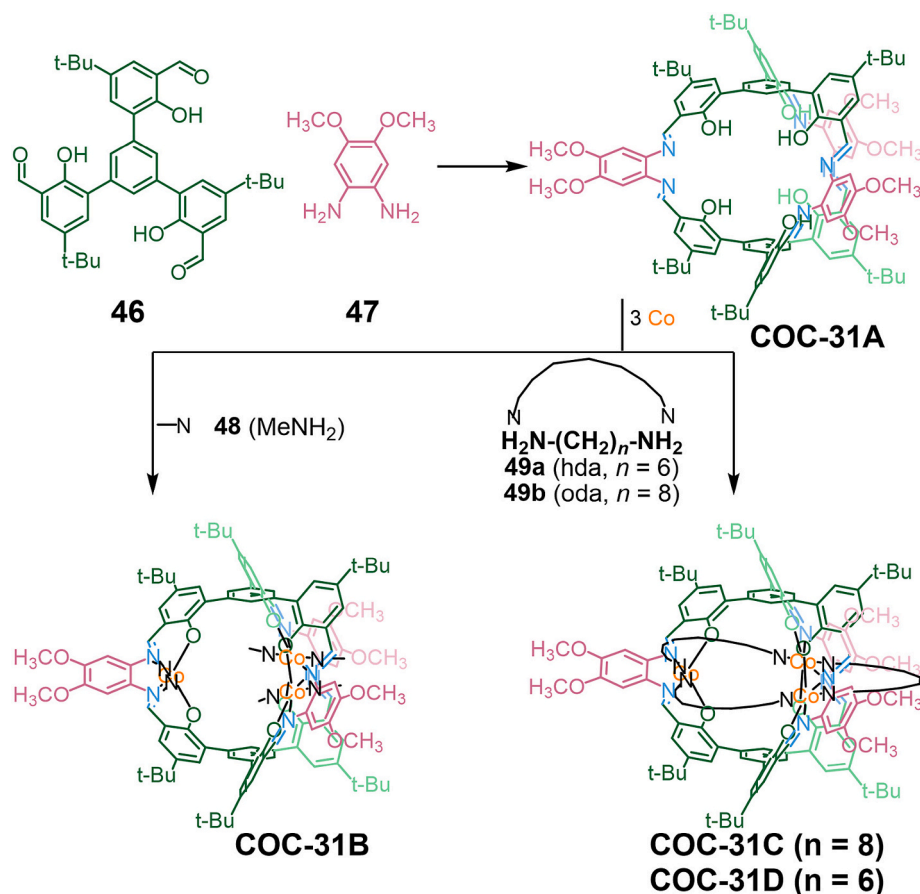


Fig. 21. Synthesis of helical imine cage **COC-31** and its aperture close through coordination.

sites can further coordinate with either longer 1,8-octanediamine (**49b**) or 1,6-hexanediamine (**49a**) ligands to immobilize the cage's apertures, resulting in **COC-31C** and **COC-31D**. In contrast, the shorter 1,4-butanediamine (**48**) is unable to bridge the cobalt(III) ion, leading to an open-shell analogue featuring a methylamine-coordinated cage, **COC-31B**. Upon evaluation, it is determined that bifunctional ligands could effectively bridge adjacent metal centers to close the apertures while also kinetically inhibiting guest uptake. The negatively polarized phenoxy group in **COC-31** exhibits a strong binding affinity for cationic species, demonstrating selectivity for larger  $\text{Cs}^+$  ions over alkali metal ions in the order  $\text{Cs}^+ > \text{Rb}^+ > \text{K}^+ \gg \text{Na}^+$ . Additionally, the **49a** ligands in **COC-31D** significantly hinder guest entry by more than three orders of magnitude due to the complete occupation of the apertures. The open-close feature of these molecular containers holds great promise for the on-demand capture and release of target species or information.

To develop a universal and efficient strategy for synthesizing more complex and multifunctional cCOCs, Prof. Zhang began exploring orthogonal dynamic covalent chemistry (ODCC) [133], and successfully prepared a new cCOC, **COC-32**, through a one-pot reaction involving Schiff base formation and olefin metathesis [59,134]. Although these two reactions are well understood, several challenges arise when attempting to execute them simultaneously in ODCC. Specifically, both primary amines and the water by-product within the Schiff base reaction can inhibit the activity of olefin metathesis catalysts [135,136]. To address this issue, they modified their approach to a sequential orthogonal reaction strategy: either (1) conducting olefin metathesis followed by the Schiff base reaction or (2) performing the Schiff base reaction first, followed by olefin metathesis. The potential inactivity of primary amines for olefin metathesis catalysts, along with incomplete deprotection of the *t*-BOC protected vinyl-substituted aniline, hindered the further Schiff base reaction. Consequently, they focused on the strategy of performing the Schiff base reaction first, followed by olefin metathesis. Subsequently, the triangular prism cage, **COC-32**, was constructed using six carbazole moieties arranged at  $90^\circ$  angles and capped with two tri-1,3,5-(4-formylphenyl)benzene units (Fig. 22) [133]. During the initial 30 min of the reaction, a successful Schiff base reaction occurs between **40** and **50** in a 1:3 ratio. Following this, the addition of Hoveyda-Grubbs second-generation catalyst facilitates olefin metathesis, yielding the desired 3D cage [59]. This work demonstrates that ODCC technology can be effectively applied to develop shape-persistent cages composed of up to three distinct building blocks. With this protocol, more complex cages with tunable sizes, shapes, and symmetries can be readily synthesized.

#### 4. cCOCs bridged by triple bond

In 1992, Prof. Wu proposed a general strategy for synthesizing nanoscale phenylacetylene cages by integrating controlled preparation of branched phenylacetylene with efficient double cyclization

[137–139]. Utilizing this approach, they initially characterize the rigid cCOCs connected by  $\text{C}\equiv\text{C}$  bonds with  $D_{3h}$  and  $C_{2v}$  symmetry, which comprised eleven and fifteen phenylacetylene repeating units, **COC-33A** and **COC-33B** (Fig. 23). The fragility of **COC-33A**'s hexagonal lamellar crystals, formed from eleven phenylacetylene units, is attributed to their high sensitivity to solvent evaporation, which hinders their potential as microporous organic solid materials [137]. Consequently, the advancement of aryl alkyne cCOCs has encountered stagnation until the alkyne metathesis method is widely adopted [32,33,96,140–142].

With the support of alkyne metathesis, an extremely effective dynamic covalent chemistry (DCC) technique [109,111,120,143,144], Prof. Zhang successfully synthesized a novel 3D rectangular cage, **COC-34**, through a single-step process using readily available porphyrin derivatives in 2011 [32]. **COC-34** consists of robust aromatic porphyrin and carbazole units interconnected by linear acetylenic connectors, which enhance its structural integrity (Fig. 24). During the chemical transformations, the linear and rigid acetylenes orient almost perpendicularly to the porphyrin ring, while the carbazole-substituted porphyrins (**52**) exhibit  $C_4$ -symmetry and maintain a fixed  $90^\circ$  angle, resulting in a cuboid architecture with minimal angular distortion. Computational modeling reveals that **COC-34** features a cavity with a height of 11.9 Å and a diameter of 18.3 Å, making it suitable for accommodating fullerenes. Remarkably, in toluene, the  $D_{4h}$ -symmetric **COC-34** forms a 1:1 complex with  $C_{60}$  and  $C_{70}$ , exhibiting high affinity constants of  $1.4 \times 10^5 \text{ M}^{-1}$  for  $C_{60}$  and  $1.5 \times 10^8 \text{ M}^{-1}$  for  $C_{70}$ . Notably, the strong interaction between **COC-34** and  $C_{70}$  allows for complete reversibility of the cage-fullerene association when subjected to acid-base stimuli, facilitating the effective isolation of  $C_{70}$  from a fullerene mixture rich in  $C_{60}$ .

The incorporation of precipitating groups into reactants is a complex process that often leads to the premature precipitation of intermediates, posing challenges for the purification of the products [32,140]. However, these precipitating groups can also enhance the reaction equilibrium and yield of DCC [145]. In the synthesis of **COC-34**, the precipitation of bis(benzoylbiphenyl)acetylene (PPT- $\text{C}\equiv\text{C}$ -PPT) by-products is a driving force; yet, this mechanism is not effective for synthesizing tetrameric cages. Prof. Zhang has developed a novel alkyne metathesis catalyst based on triphenolsilane [31,146]. By utilizing 5 Å molecular sieves to absorb the by-product 2-butyne, this catalyst efficiently promotes the alkyne metathesis of propynyl-modified monomers in an isolated system, achieving a high conversion yield. They designed a  $C_3$ -symmetric trialkyne precursor (**53**) to synthesize the expected  $T_d$ -symmetric tetrameric cages, **COC-35**, through alkyne metathesis at  $55^\circ\text{C}$ . However, the reaction yielded  $D_{2h}$ -symmetric **COC-36** instead, due to the edge-plane angle of  $60^\circ$  in **53** matching the tetrahedron's edge-plane angle of  $54.7^\circ$  [140]. Attempts to perform cross-coupling between Br-terminated and alkyne-terminated components to synthesize **COC-36** were unsuccessful, underscoring the advantages of a dynamic covalent approach over kinetically regulated methods for constructing

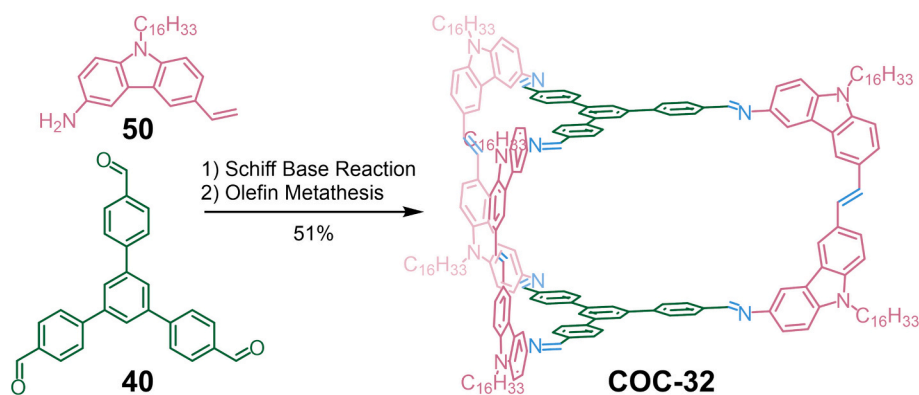


Fig. 22. Construction of double bond linked **COC-32** via orthogonal Schiff base reaction and olefin metathesis.

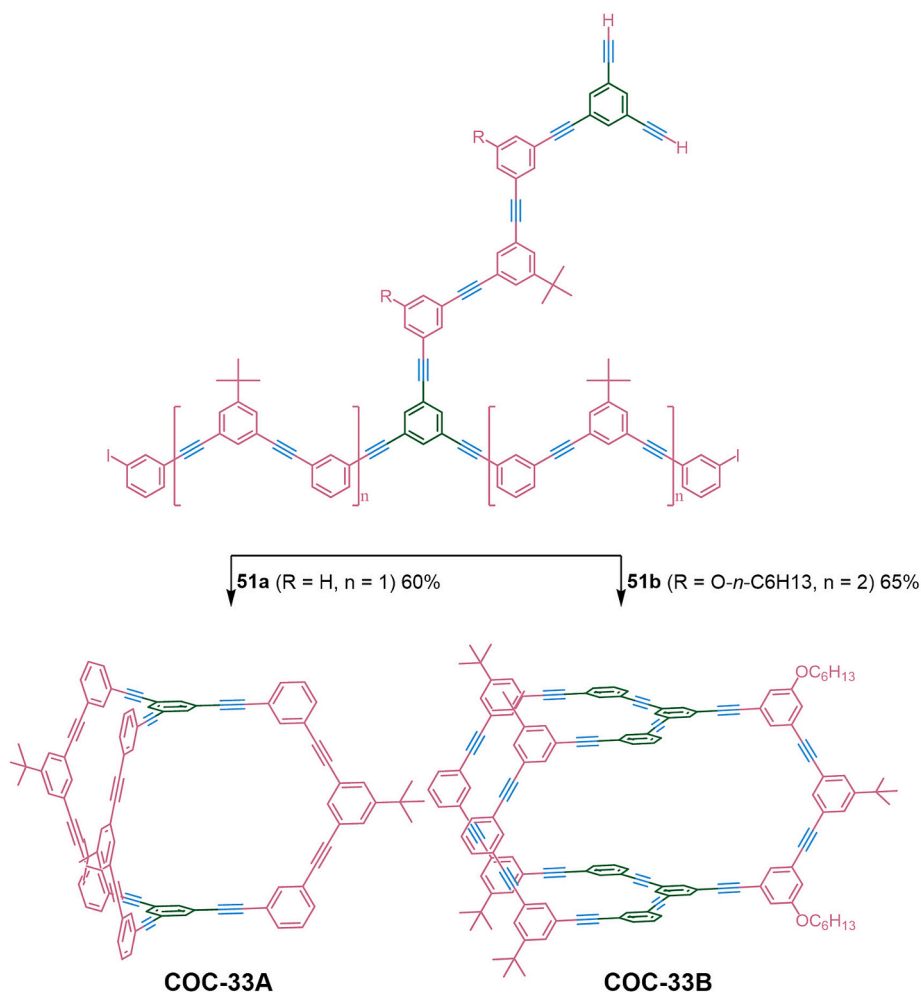


Fig. 23. Construction of alkyne COC-33 through intramolecular Sonogashira coupling reaction.

complex molecular structures. Furthermore, **COC-36A** demonstrates a preferred association with  $C_{70}$  ( $K = 3.9 \times 10^3 \text{ M}^{-1}$ ) while showing no significant association with  $C_{60}$ .

Building on the tetrameric cage, Prof. Zhang was inspired to design and synthesize a series of self-reactive tritopic building blocks as monomers with  $C_3$  symmetry, aiming to construct interlocked arylene ethynylene cages through alkyne metathesis. The equilibrium conversion of **54** and **55** into monomeric cage **COC-37/COC-38** and catenane cage **COC-37C/COC-38C** was achieved by precipitating the by-product PPT-C $\equiv$ C-PPT using a highly active multidentate molybdenum carbyne complex as the catalyst [31,142]. The reaction progression is analyzed at various time points using gel permeation chromatography (GPC) and matrix-assisted laser desorption/ionization time-of-flight mass spectrometry (MALDI-MS) to investigate the formation of the catenane **COC-37C**. The results reveal that within 30 min, catenane cages predominately form due to the high initial monomer concentration, suggesting that the generation of monomeric cages and catenane cages occurs concurrently. It appears that the thermodynamic preference for the catenane cage is higher than that for the monomeric cage. The exceptional stability and ability to produce interlocked products suggest that this template-free method may be valuable for constructing polycatenanes with significantly enhanced flexibility and robustness, attributed to the ethynylene connections.

To enhance the understanding of the relationship between the architectures of rigid ethynylene-based cCOCs synthesized via alkyne metathesis and the geometries of their constituent units, Prof. Zhang conducted a comprehensive review of relevant studies [141]. They

investigated the synthesis of the monomeric cage **COC-34** and the catenane cages **COC-37C** and **COC-38C** through a one-step alkyne metathesis of multi-alkyne monomers. These building blocks feature dual plates (faces) and numerous symmetrically arranged carbazole arms (edges), with an angle close to  $90^\circ$  between the faces and edges. The triphenylbenzene-based monomers (**54** and **55**) predominantly form catenane structures **COC-37C** and **COC-38C** (59 %), while only a minor amount of the monomeric cage (6 %) is produced. In contrast, the porphyrin-based monomer yields a significant quantity of **COC-34** (72 %) without the formation of notable interlocked species [32,142]. Intrigued by these findings, they modified the central core of the monomer by substituting it with a benzene ring to create **56** terminated with PPT [32,140,142,145]. The alkyne metathesis of **56** resulted in the formation of the  $D_{2h}$ -symmetric tetrameric cage **COC-39**, rather than the anticipated dimeric cage **COC-40** [141]. Subsequently, they extended the monomer's plate to include triphenylamine and tetraphenylporphyrin, incorporating tri- and tetra-carbazolyl moieties while maintaining fixed face-to-face angles of  $90^\circ$ . A molybdenum carbyne catalyst containing triphenol silane was employed for the alkyne metathesis. Notably, the symmetric dimer **COC-41** was produced in an excellent isolated yield of 84 % from the triphenylamine-based monomer (**57**), contrary to the expected  $D_{2h}$  symmetric tetramer. In the case of the tetraphenylporphyrin-based monomer, unknown precipitates were obtained, with only trace amounts of a dimer species observed in the crude mixture via MALDI-MS. The impact of the size and geometry of the building blocks on the assembly process was systematically investigated through a re-examination of the design and synthesis of

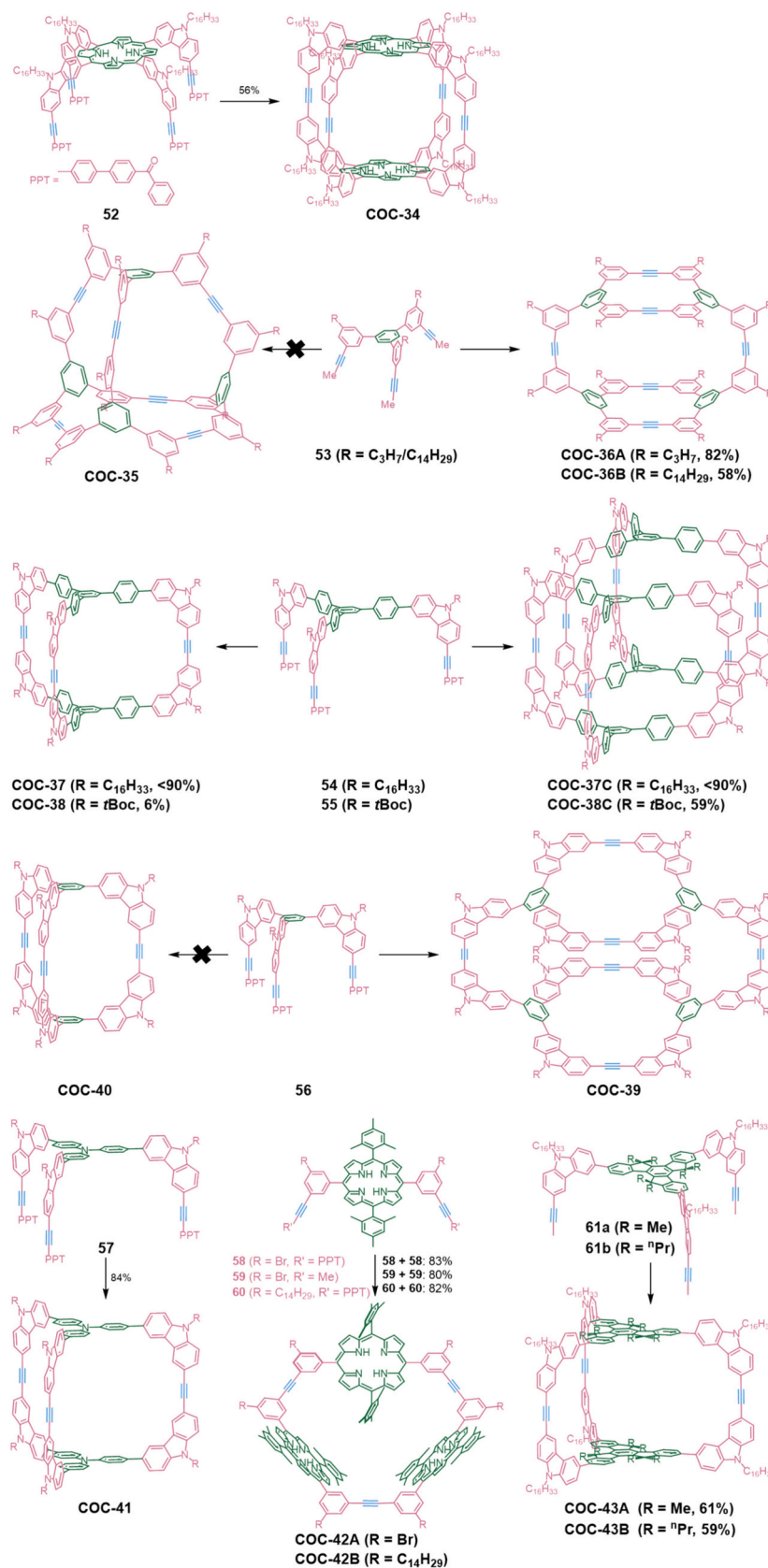


Fig. 24. Construction of alkyne cCOCs, COC-34 ~ COC-43, through alkyne metathesis.

aryleneethynylene cages **COC-N** (where  $N = 34, 36, 37C, 38C, 40, 41$ ) via dynamic alkyne metathesis. The findings suggest two key insights: (1) The geometry and size of the monomer significantly influence the dynamic process of alkyne metathesis and the final topology of the cage; and (2) There is an inevitable kinetic competition between intra- and intermolecular metathesis that affects the cage topology for multi-alkyne monomers. Intramolecular metathesis is more favorable for dimerization, leading to the formation of dimeric cages. Consequently, the formation of tetrameric cCOCs through intermolecular metathesis is kinetically disfavored (as seen in **COC-35**); however, if a strong thermodynamic preference exists, it may dominate.

The methodology established in 2015 for synthesizing the cyclic porphyrin trimer **COC-42** utilized alkyne metathesis [96]. Three symmetric porphyrin monomers were specifically designed and synthesized for the cyclic trimers, **COC-42A** (with  $R = \text{Br}$ ) and **COC-42B** (with  $R = \text{C}_{14}\text{H}_{29}$ ), through alkyne metathesis using an in situ generated molybdenum catalyst [96,145,146]. The desired product, **COC-42A**, was obtained in highly isolated yields from either the PPT- or methyl-substituted monomer (**58** or **59**, 83 % and 80 %, respectively). Monomer **60** also yielded **COC-42B** with a commendable yield of 82 %, along with enhanced solubility, utilizing the precipitation-driven alkyne metathesis approach. The Zn metalated derivative, **Zn-COC-42A**, was readily prepared from **COC-42A** with a high yield of 93 %. When exposed to fullerenes, **Zn-COC-42A** exhibits intriguing host-guest interactions, demonstrating a marked preference for associating with  $\text{C}_{70}$  ( $6 \times 10^3 \text{ M}^{-1}$ ) over  $\text{C}_{84}$  and  $\text{C}_{60}$  (not detected). The captured  $\text{C}_{70}$  in the integrated complex  $\text{C}_{70}@\text{Zn-COC-42A}$  could be released through an exchange reaction with 2,4,6-tri(4-pyridyl)-1,3,5-triazine. Additionally, another guest exchange process occurs when **COC-34**, which has a greater binding affinity for  $\text{C}_{70}$ , is introduced into the solution of  $\text{C}_{70}@\text{Zn-COC-42A}$ .

Prof. Zhang is dedicated to synthesizing innovative cCOCs with strong electron-donating capabilities for guest encapsulation. As such, they have designed and synthesized  $\text{C}_{3h}$ -symmetric monomers, **61a** and **61b**, integrating truxene [147–150], carbazole, and propargyl moieties. To enhance solubility during the reaction and to prevent the premature formation of large intermediate oligomers and polymers before achieving the desired product, alkyl groups have been introduced into the carbazole and truxene moieties. **COC-43A** and **COC-43B** were obtained in high yields through one-step alkyne metathesis [33]. Significantly, the interaction between fullerenes and **COC-43** is investigated through photoluminescence (PL) titration experiments, revealing a high binding constant of  $10^5 \text{ M}^{-1}$ . The complexation of  $\text{C}_{70}@\text{COC-43A}$  is exothermic, with an enthalpy change of  $-102.7 \text{ kJ}\cdot\text{mol}^{-1}$  as determined by DFT calculations. Overall, the thermodynamics of the system drive the complexation process, indicating potential applications as discrete fullerene acceptors. The utilization of such donor-acceptor complexation systems may offer significant benefits for optoelectronic applications and artificial photosynthetic systems.

Concurrently, Prof. Servalli has employed classical coupling techniques to synthesize novel alkyne-based cCOCs with anthracene, **COC-44**, and to investigate their crystal structures (Fig. 25) [34]. The synthesis of anthracene-1,8-ditriflate has been successfully achieved using a modified three-step process starting from 1,8-dihydroxyanthraquinone, resulting in an overall yield of up to 71 % at a scale of 15 g within one week. An excess of anthracene-1,8-ditriflate was then reacted with 1,3,5-triynylidenebenzene under standard Sonogashira conditions, leading to the formation of the [3 + 1] intermediate (**62**) in moderate yield. The target cage **COC-44** was then obtained through copper-free Sonogashira coupling in high dilution conditions using equimolar amounts of **62** and 1,3,5-triynylidenebenzene. **COC-44** exhibits a remarkable propensity for crystallization with size of 100–200  $\mu\text{m}$  in fourteen distinct solvents. SC-XRD analysis reveals that **COC-44** adopts layered structures regardless of the solvent used for crystallization. However, the choice of solvent may influence the packing arrangement within these layers, leading to different interactions among the

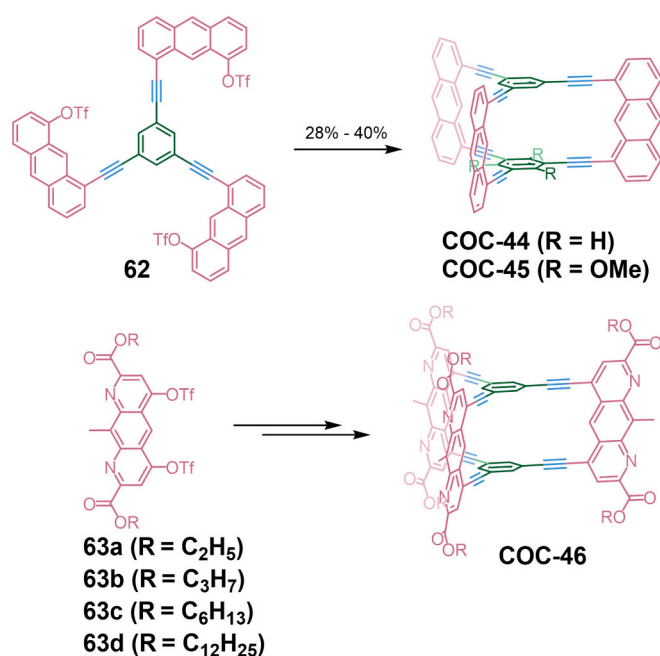


Fig. 25. Synthesis of alkyne **COC-44** ~ **COC-46** through stepwise Sonogashira coupling reaction.

anthracene units in **COC-44** [34,53]. The predominant interactions identified are edge-to-face  $\text{CH}\cdots\pi$  interactions, with some solvates also demonstrating partial face-to-face  $\pi\cdots\pi$  interactions in addition to the edge-to-face  $\text{CH}\cdots\pi$  interactions. This specific packing is most frequently observed with solvents capable of inducing a planar conformation or those exhibiting acceptor character. Qualitative analysis reveals a strong negative surface potential on the anthracene faces, which may explain why anthracene tends to avoid face-to-face  $\pi\cdots\pi$  interactions. These results provide valuable insights into strategies for achieving all-face-to-face packing, which is favorable for single-crystal transformations.

Throughout this period, Prof. Servalli has focused on advancing the crystallization and stacking behavior of **COC-44**. Among the seven identified primary packing motifs, three exhibited photoreactivity [53]. This led to the successful synthesis of the new linear polymer, [4 + 4]-cycloaddition dianthraphane, and poly<sub>1D</sub>anthraphane through a quantitative single-crystal-to-single-crystal (SCSC) transformation [54]. To minimize misalignment in the anthracene pairs within the crystals, a trimethoxy-substituted triethynylbenzene moiety was introduced, resulting in the formation of **COC-45**. This cage crystallize into distinct plates under the same synthetic conditions as **COC-44** [34,55]. During the crystallization of **COC-45** in various solvents, two novel packing motifs are generated: edge-to-face and photoreactive edge-to-face/face-to-face configurations. The radiation-induced [4 + 4]-cycloaddition of the face-to-face stacked anthracene units in the single crystals of the edge-to-face/face-to-face packing leads to a SCSC linear photopolymerization, producing single crystals of poly<sub>1D</sub>anthraphane-tri (OMe). The nearly perfect stacking of the anthracene pairs facilitates smooth and rapid polymerization with minimal alterations to the crystal parameters. Moreover, this study reveals an unprecedented case of polyanthracene isomerism, where the dimerization reaction can yield either *endo,endo*- or *exo,exo*-configured polymers, depending on the orientation of the anthracene units involved. The isomerism results in chains in the *exo,exo* polymer being approximately 26 % thicker ( $\sim 30.1 \text{ \AA}$ ) than those in the *endo,endo* instance ( $\sim 23.8 \text{ \AA}$ ). Additionally, the *exo,exo* polymer is about 20 % shorter than the *endo,endo* variant. This variation may influence chain solubility and potentially alter the architectural range of polyanthracenes. Given that this growth chemistry could pave the way for 2D materials, they are committed to extending this [4 + 4] cycloaddition protocol to 1,8-diazoanthracene

moiety (**63a** ~ **63d**). This extension aims to synthesize a series of new  $D_{3h}$ -symmetric propeller-shaped cages, designated as **COC-46** [56]. Considering the stability of its molecular geometry, a face-to-face arrangement is anticipated [34,55,56].

## 5. cCOCs bridged by single atoms

In addition to the previously mentioned cCOCs connected by conjugated chemical bonds, there exists a distinct category of cCOCs that feature single atoms for conjugation. Most of the aforementioned cCOCs exhibit a relatively limited extent of  $\pi$ -conjugation. On one hand, each bridge acts as a local site of  $\pi$ -conjugation, which is disrupted at the bonding site [20,22,52,60,137]. On the other hand, the significant dihedral angles between the bridges and the aromatic plates lead to weakened  $\pi$ -conjugation [32]. Recently developed C/N-centered complete fusion cages demonstrate an enhanced degree of conjugation compared to the previously mentioned cCOCs, facilitating efficient 3D electron delocalization. These diverse cCOCs, characterized by their unique structures, symmetries, and spin states, contribute to our understanding of electron and spin interactions in 3D space. They also provide valuable insights into the concept of 3D global  $\pi$ -aromaticity.

### 5.1. Carbon centered cCOCs

cCOCs with radical features exhibit significantly enhanced conjugation, which is crucial for the development of molecular magnets in 2D/3D architectures. Prof. Wu successfully synthesized the first biradical **COC-47** in 2017 [35]. The synthesis of **COC-47** involved intermolecular Suzuki coupling, bromination, Yamamoto homo-coupling, and oxidation (Fig. 26). X-ray crystallography reveals that in **COC-47**, the three tetrachlorophenyl units at each bridgehead of the cage adopt a propeller geometry, with the bridgehead carbons being  $sp^2$ -hybridized. The twist angles between adjacent carbazole units are  $23.3^\circ$ ,  $25.9^\circ$ , and  $32.9^\circ$ , respectively. The mean torsional angle between the carbazole and tetrachlorophenyl units is approximately  $65.8^\circ$ , indicating an asymmetric structure with one arm exhibiting a significantly different twist angle compared to the other. In the crystal structure of **COC-47**, two enantiomers are present: “P,” which rotates in a clockwise manner, and “M,” which rotates counterclockwise. Both enantiomers of the polychlorotriphenylmethyl (PTM) subunits exhibit identical helicity. Each **COC-47** cage is surrounded by four nearest neighbors in a body-centered

cubic arrangement. Within the crystal, close contacts involving  $[\text{CH}\cdots\pi]$  and  $[\text{CH}\cdots\text{Cl}]$  interactions are observed between the enantiomers, although no  $\pi$ - $\pi$  interactions between neighboring cages are detected. **COC-47** displays three distinct resonance forms. Crystal form A: Free electrons are confined within the isolated PTM fragments. Crystal form B: An intramolecular charge transfer (ICT) occurs from the carbazole donor to the PTM acceptor, resulting in a zwitterionic state. Crystal form C: A fully paired quinonal dication is formed through an antiferromagnetic coupling process between adjacent aminyl radical cations. These three resonance forms are present in each bridge, dispersing charge and spin throughout the entire skeleton. The 3D global  $\pi$ -conjugation has been confirmed through various characterizations, including DFT and ACID calculations. Polar solvents like DMF can stabilize the zwitterionic form resulting from ICT. The distorted structure and a distance of 9.943 Å between the bridgehead carbons contribute to weak interactions between the two PTM radicals.

### 5.2. Nitrogen centered cCOCs

Triphenylamine compounds can be integrated into cCOCs due to their rigid structure, high spin alignment, and continuous  $\pi$  conjugation [151–153]. Cylindrical cCOCs were synthesized using iterative Buchwald-Hartwig cross-coupling reactions involving triphenylamine derivatives (**66** and **67**) (Fig. 27) [36]. This study presents the first determination of cCOCs with an N-centered structure via X-ray crystallography. The  $C_3$ -symmetric bilayer structure of **COC-48A** features six anisyl groups, with two benzene rings as decks that are spaced 4.77 Å apart. The dihedral angle between the 1,3,5-phenylenetriamine surface and the *meta*-phenylene faces is approximately  $76$ – $80^\circ$ . Additionally, reversible multiredox activity is observed in the bilayer cage **COC-48B**, which is decorated with six *N*-dianisylaminophenyl groups. The synthesis of trilayer **COC-49** has also been accomplished, revealing a  $C_3$ -symmetrical triple-decker structure akin to that of **COC-48A**, but with notably longer distances (4.84 Å) between the cofacial benzene decks and nearly perpendicular *meta*-phenylene pillars relative to the 1,3,5-benzenetriamine planes.

Following the initial discovery of the first carbon-centered diradical cCOC, **COC-47**, Prof. Wu has reported several cCOCs with diverse conjugated backbones [28,29,45,123]. Recently, to explore the intricate relationship between 2D Hückel/Baird aromaticity and 3D global aromaticity [28,47], they focused on an intriguing conjugated unit, dimethylmethylene-bridged triphenylamine (DTPA). This unit can

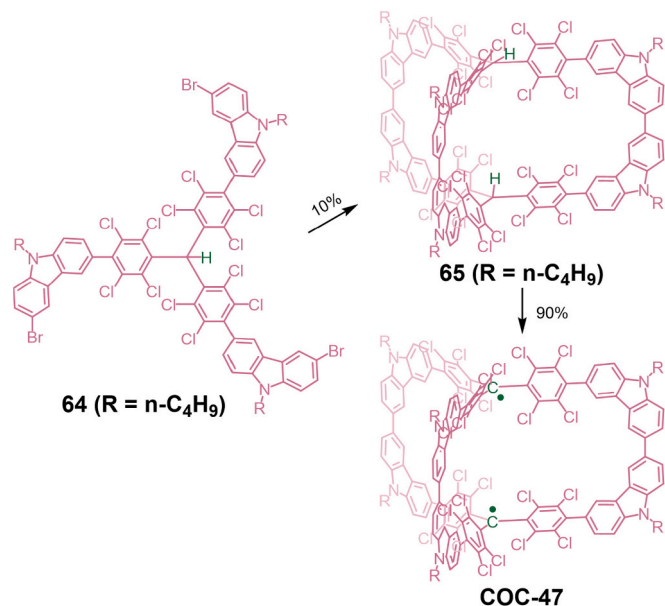


Fig. 26. Synthesis of carbon radical centered **COC-47**.

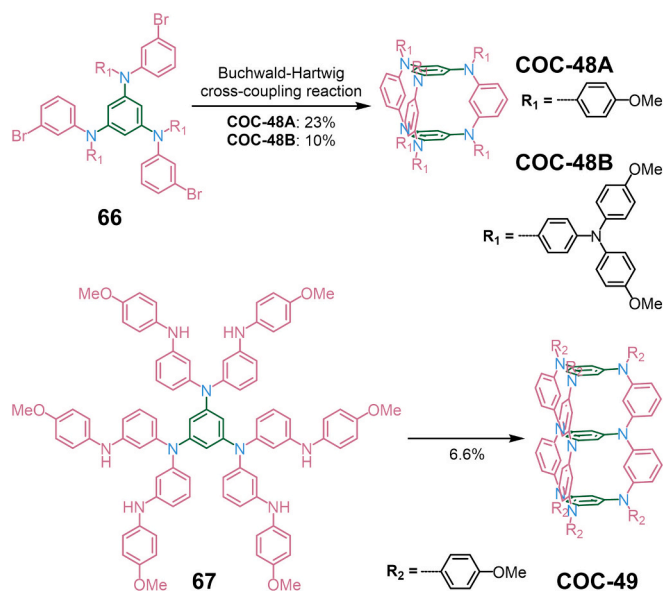


Fig. 27. Synthesis of triarylamine cCOCs, **COC-48** and **COC-49**.

undergo oxidation to form stable radical cations, which facilitate electron (spin) interactions that enhance 3D electron delocalization. They designed tetrahedral-like cCOCs with  $T_d$  symmetry through coupling of pinacol borate trisubstituted DTPA (**68**) (Fig. 28). However, they unexpectedly obtained an open cage, **COC-50**, with reduced symmetry [48]. Additionally, they synthesized *trans*- and *cis*- macrocyclic trimers, **70** and **71**, for comparative analysis. Both experimental results and theoretical analyses reveal several key findings: (1) **COC-50** exhibits a robust electron absorption band at 361 nm in dichloromethane, with no substantial alteration in the bond lengths of C—C and C—N. This consistency with the typical bond lengths associated with the DTPA building unit indicates weak  $\pi$ -electron delocalization and localized aromaticity within the isolated benzene rings of the **COC-50** skeleton. (2) The radical cation **COC-50**<sup>+</sup>·**SbCl<sub>6</sub>**<sup>−</sup> displays strong and broad optical absorption features, peaking at 361, 1000, and 2000 nm, and extending beyond 2800 nm. Although there is a slight reduction in the harmonic oscillator model of aromaticity (HOMA) value for the benzene rings in the cage skeleton, this suggests a strengthened  $\pi$ -electron delocalization based on slightly shorter C—N bonds in the DTPA arms compared to **COC-50**. (3) Similarly, the compound **COC-50**<sup>2+</sup>·**2SbF<sub>6</sub>**<sup>−</sup> shows strong and broad optical absorption, peaking at 474 and 904 nm and extending beyond 1600 nm. A bicyclic (anti)aromaticity is noted in **COC-50**<sup>2+</sup>·**2SbF<sub>6</sub>**<sup>−</sup>, featuring one aromatic macrocycle (38 $\pi$ ) and one anti-aromatic macrocycle (28 $\pi$ ). In contrast, the compounds **18**<sup>2+</sup>·**2SbF<sub>6</sub>**<sup>−</sup> and **19**<sup>2+</sup>·**2SbF<sub>6</sub>**<sup>−</sup> are found to be globally antiaromatic and nonaromatic, respectively. (4) In one of the macrocycles (36 $\pi$ ), **COC-50**<sup>4+</sup>·**4SbF<sub>6</sub>**<sup>−</sup> exhibits significant 2D Hückel antiaromaticity. Moreover, **COC-50**<sup>2+</sup>·**2SbF<sub>6</sub>**<sup>−</sup>, **COC-50**<sup>4+</sup>·**4SbF<sub>6</sub>**<sup>−</sup>, and **18**<sup>2+</sup>·**2SbF<sub>6</sub>**<sup>−</sup> present a ground state characterized by an open-shell singlet with distinct diradical character, while **19**<sup>2+</sup>·**2SbF<sub>6</sub>**<sup>−</sup> adopts a triplet ground state to alleviate strain. These findings underscore the complexity of aromaticity in asymmetric cCOCs, where the (anti)aromaticity of neighboring macrocycles can influence one another. Consequently,  $\pi$ -electrons may preferentially delocalize across one or more macrocycles, satisfying different aromatic criteria. Unlike higher-symmetry cCOCs, the  $\pi$ -electrons in asymmetric cCOCs tend to spread across individual macrocycles, resulting in overall aromatic or antiaromatic behavior in three dimensions.

They also developed a novel N-centered cCOC, **COC-51**, which consists of two DTPA units and three quinooidal bithiophene arms. This structure was synthesized through intermolecular Yamamoto coupling followed by reductive aromatization (Fig. 29) [49]. **COC-51** can exist in various valence states achieved through oxidation. The non-planar conformation of DTPA induces strain, resulting in the three bithiophene arms, labeled  $\alpha$ ,  $\beta$ , and  $\gamma$ , exhibiting distinct bond lengths of 1.367

Å, 1.376 Å, and 1.355 Å, respectively. Based on detailed measurements and calculations, the following observations are made: (1) The monocyclic combinations  $\alpha\beta$ ,  $\alpha\gamma$ , and  $\beta\gamma$  in **COC-51** display HOMA values of 0.40, 0.36, and 0.33, indicating overall non-aromatic properties. In contrast, **COC-51**<sup>6+</sup> exhibits larger HOMA values (0.65) across all three macrocycles. This increase can be attributed to the greater number of aromatic rings per macrocycle in **COC-51**<sup>6+</sup> (which contains four benzene and four thiophene rings) as opposed to **COC-51** (which has only four benzene rings). (2) For **COC-51**<sup>2+</sup>, the calculated HOMA values are 0.70 (for the  $\alpha\beta/\beta\alpha'$  pair) and 0.68 (for  $\alpha\alpha'$ ), significantly exceeding those of **COC-51**. These values indicate that each macrocycle is 2D aromatic, adhering to the primary 38  $\pi$ -electron count while satisfying Hückel's [4N + 2] aromaticity rule. Consequently, **COC-51**<sup>2+</sup>, with  $D_3$  symmetry in an open singlet ground state and a conjugated skeleton comprising 56  $\pi$ -electrons, demonstrates global aromaticity according to the [6N + 2] rule. (3) The  $D_3$ -symmetric **COC-51**<sup>4+</sup>, in a triplet ground state, also exhibits 2D aromaticity in line with the [6N] electron rule. The entire 54  $\pi$ -electron skeleton shows global 3D aromaticity. The HOMA values of 0.74 (for  $\alpha\beta/\beta\alpha'$ ) and 0.63 (for  $\alpha\alpha'$ ) suggest that each macrocycle adheres to a predominant 36 $\pi$  conjugation, satisfying the Baird [4N] aromatic rule. This study, in conjunction with previous research, provides new insights into the intricate relationship between 2D Hückel/Baird aromaticity and 3D global aromaticity. It posits that global aromatic cages in three dimensions can be likened to "poly (macrocyclic) aromatic hydrocarbons" in two dimensions [28,29,45,47].

## 6. Conclusion and outlook

Conjugated cage chemistry has become a vibrant area of research, captivating chemists around the globe and leading to significant advancements in recent years. These breakthroughs have resulted in a diverse array of structurally complex and novel cCOCs. To better understand and categorize these newly discovered compounds, we have organized them based on their bridging structures of the cCOCs, resulting in four distinct categories: cCOC bridged by single bonds, double bonds, triple bonds, and single atoms. Each category represents a unique class of cCOCs, characterized by specific properties and potential applications. In addition to these categorizations, we have conducted a comprehensive analysis of the synthetic strategies employed in the creation of these novel cCOCs over the past decade. (1) cCOCs Bridged by Single Bonds: These can be synthesized through several methods, including the aromatization of strain buffers (such as 3,6-*syn*-dimethoxy-cyclohexa-1,4-diene, *cis*-1,4-diphenylcyclohexane, and ethylene), metal templating, and multiple coupling reactions. (2) cCOCs Bridged by Double Bonds: These compounds can be obtained via various reactions, including the Wittig reaction, Knoevenagel reaction, resonance aromatization (involving phenylmethene, thiophenemethene, and pyrromethene), olefin metathesis, the Perkin reaction, and Schiff-base reactions. Notably, they exhibit abundant global aromaticity in various oxidized states. (3) cCOCs Bridged by Triple Bonds: These can be synthesized using alkyne metathesis or Sonogashira coupling reactions, demonstrating excellent host-guest capabilities. (4) cCOCs Bridged by Single Atoms: These include structures utilizing carbon radicals and nitrogen, which can also be synthesized effectively. Each of these synthetic strategies possesses unique advantages and applications, contributing to the growing diversity of cCOCs and paving the way for new research avenues in the field of conjugated cage chemistry.

Despite the significant advancements in the design and synthesis of cCOCs, several pressing challenges remain that require immediate attention: (1) Suboptimal Synthetic Strategies and Yields: Current synthetic strategies for cCOCs are far from optimal. DCC offers a robust platform for the efficient construction of cCOCs with novel linkages. Various DCC approaches, including alkyne metathesis, olefin metathesis, the Knoevenagel reaction, and imine reaction, have been successfully employed to synthesize cCOCs. However, the precise mechanism

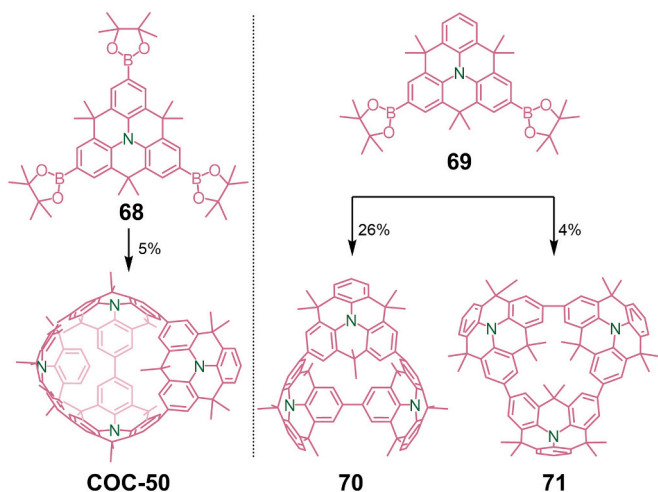


Fig. 28. Synthesis of DTPA based cCOC, **COC-50**.

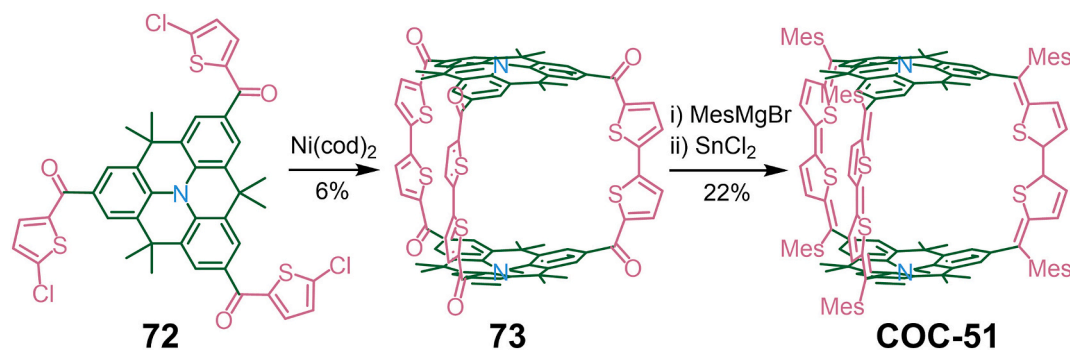


Fig. 29. Synthesis of DTPA capped cCOC, COC-51.

for using dynamic alkyne metathesis in the preparation of cCOCs remains elusive due to the intricate interplay of factors such as catalysts, building blocks, thermodynamic stability, and kinetic control. Moreover, the stability of imine-based cCOCs is inadequate for thorough research and subsequent applications. Therefore, there is an urgent need to develop novel DCC approaches to efficiently construct cCOCs with unique structures. Additionally, multiple compound reactions (MCRs) represent another potential strategy for constructing cCOCs with a more abundant range of structures. cCOCs linked through rising or mixed conjugated units, such as azo, ene-yne, and diyne, could significantly expand their structural diversity. (2) Expansion of Structural Scope: Aromaticity and host-guest interactions are crucial elements for the optoelectronic properties of cCOCs and their interaction with the external environment. The composition of cages can greatly benefit from a strategic selection of building blocks. This includes the incorporation of heteroatoms, such as metal ions, to reduce symmetry, integrate responsive moieties, and combine bridging units. Additionally, employing interlocking techniques or post-synthetic modification (PSM) can enhance the complexity of the structures. The topologies of these cages can be finely tuned through geometric matching of building blocks and the orientation of bonds in the formed linkages. These strategies open up a wealth of opportunities for the creation of newly diverse cCOC architectures.

Ultimately, the properties and practical applications of cCOCs represent the paramount goal of cCOC chemistry. Their optoelectronic properties are particularly noteworthy, as they significantly influence the potential applications of these materials in the field of optoelectronics. The rich optoelectronic characteristics of cCOCs could drive the development of innovative devices and technologies, paving the way for a wide range of practical applications in areas such as energy conversion, information processing, and display technologies. Furthermore, cCOCs can serve as promising precursors for constructing branched nanocarbons using appropriate methods. The synthesis of these branched nanocarbons from cCOCs is an emerging area of research that holds great promise for developing new materials with unique properties.

In summary, despite the challenges that remain in the design and synthesis of cCOCs, the potential benefits of these materials warrant further investigation. By addressing these challenges and gaining a deeper understanding of the complex interactions between cCOCs and their guests, researchers can leverage diverse host-guest interactions for applications in absorption, separation, complexation, and other practical uses across various fields.

#### Declaration of competing interest

The authors declare that they have no known competing financial interests or personal relationships that could have appeared to influence the work reported in this paper.

#### Data availability

Data will be made available on request.

#### Acknowledgments

This work was supported by the Class III Peak Discipline of Shanghai-Materials Science and Engineering (High Energy Beam Intelligent Processing and Green Manufacturing), and Fundamental Research Funds for the Central Universities (YG2023QNA04 and YG2022QN027).

#### References

- [1] A. Pron, P. Gawryls, M. Zagorska, D. Djurado, R. Demadrille, Electroactive materials for organic electronics: preparation strategies, structural aspects and characterization techniques, *Chem. Soc. Rev.* 39 (2010) 2577, <https://doi.org/10.1039/b907999h>.
- [2] N. Blouin, M. Leclerc, Poly(2,7-carbazole)s: structure–property relationships, *Acc. Chem. Res.* 41 (2008) 1110–1119, <https://doi.org/10.1021/ar800057k>.
- [3] C. Wang, H. Dong, W. Hu, Y. Liu, D. Zhu, Semiconducting  $\pi$ -conjugated systems in field-effect transistors: a material odyssey of organic electronics, *Chem. Rev.* 112 (2012) 2208–2267, <https://doi.org/10.1021/cr100380z>.
- [4] W. Wu, Y. Liu, D. Zhu,  $\pi$ -Conjugated molecules with fused rings for organic field-effect transistors: design, synthesis and applications, *Chem. Soc. Rev.* 39 (2010) 1489–1502, <https://doi.org/10.1039/B813123F>.
- [5] R.L. McRae, R.L. Phillips, I.-B. Kim, U.H.F. Bunz, C.J. Fahrni, Molecular recognition based on low-affinity polyvalent interactions: selective binding of a carboxylated polymer to fibronectin fibrils of live fibroblast cells, *J. Am. Chem. Soc.* 130 (2008) 7851–7853, <https://doi.org/10.1021/ja8007402>.
- [6] K. Li, J. Pan, S. Feng, A.W. Wu, K. Pu, Y. Liu, B. Liu, Generic strategy of preparing fluorescent conjugated-polymer-loaded poly(DL-lactide-co-Glycolide) nanoparticles for targeted cell imaging, *Adv. Funct. Mater.* 19 (2009) 3535–3542, <https://doi.org/10.1002/adfm.200901098>.
- [7] X. Chen, S. Lenhart, M. Hirtz, N. Lu, H. Fuchs, L. Chi, Langmuir–Blodgett patterning: a bottom-up way to build mesostructures over large areas, *Acc. Chem. Res.* 40 (2007) 393–401, <https://doi.org/10.1021/ar600019r>.
- [8] A.R. Tao, J. Huang, P. Yang, Langmuir–Blodgett of nanocrystals and nanowires, *Acc. Chem. Res.* 41 (2008) 1662–1673, <https://doi.org/10.1021/ar8000525>.
- [9] T. He, K. Geng, D. Jiang, All  $sp^2$  carbon covalent organic frameworks, *Trends Chem.* 3 (2021) 431–444, <https://doi.org/10.1016/j.trechm.2021.03.008>.
- [10] X. Li,  $sp^2$  carbon-conjugated covalent organic frameworks: synthesis, properties, and applications, *Mater. Chem. Front.* 5 (2021) 2931–2949, <https://doi.org/10.1039/D1QM00015B>.
- [11] C.D. Dimitrakopoulos, P.R.L. Malenfant, Organic thin film transistors for large area electronics, *Adv. Mater.* 14 (2002) 99–117, [https://doi.org/10.1002/1521-4095\(20020116\)14:2<99::AID-ADMA99>3.0.CO;2-9](https://doi.org/10.1002/1521-4095(20020116)14:2<99::AID-ADMA99>3.0.CO;2-9).
- [12] L. Guo, Z. Wu, Y. Liang, Nanotubes of poly(phenylene vinylene) derivative at the air/water interface, *Chem. Commun.* (2004) 1664–1665, <https://doi.org/10.1039/B403870C>.
- [13] E. Meirzadeh, A.M. Evans, M. Rezaee, M. Milich, C.J. Dionne, T.P. Darlington, S. T. Bao, A.K. Bartholomew, T. Handa, D.J. Rizzo, R.A. Wiscons, M. Reza, A. Zangiabadi, N. Fardian-Melamed, A.C. Crowther, P.J. Schuck, D.N. Basov, X. Zhu, A. Giri, P.E. Hopkins, P. Kim, M.L. Steigerwald, J. Yang, C. Nuckolls, X. Roy, A few-layer covalent network of fullerenes, *Nature* 613 (2023) 71–76, <https://doi.org/10.1038/s41586-022-05401-w>.
- [14] V.B. Mbayachi, E. Ndayiragije, T. Sammani, S. Taj, E.R. Mbata, A.U. Khan, Graphene synthesis, characterization and its applications: a review, *Results Chem.* 3 (2021) 100163, <https://doi.org/10.1016/j.rechem.2021.100163>.
- [15] Y.-J. Shen, K.-L. Zhu, J.-Q. Liang, X. Sun, H.-Y. Gong, Carbon-rich macrocycles and carbon nanoribbons as unique optical materials, *J. Mater. Chem. C* 11 (2023) 4267–4287, <https://doi.org/10.1039/D2TC05492B>.

- [16] M.J. Strauss, A.M. Evans, E.K. Roesner, R.J. Monsky, M.I. Bardot, W.R. Dichtel, Divergent nanotube synthesis through reversible macrocycle assembly, *Acc. Mater. Res.* 3 (2022) 935–947, <https://doi.org/10.1021/accountsmr.2c00062>.
- [17] M.J. Strauss, M. Jia, A.M. Evans, I. Castano, R.L. Li, X. Aguilar-Enriquez, E. K. Roesner, J.L. Swartz, A.D. Chavez, A.E. Enciso, J.F. Stoddart, M. Rolandi, W. R. Dichtel, Diverse proton-conducting nanotubes via a tandem macrocyclization and assembly strategy, *J. Am. Chem. Soc.* 143 (2021) 8145–8153, <https://doi.org/10.1021/jacs.1c02789>.
- [18] L. Li, C. Zhang, L. Xu, C. Ye, S. Chen, X. Wang, Y. Song, Luminescence ratiometric nanothermometry regulated by tailoring annihilators of triplet–triplet annihilation upconversion nanomicelles, *Angew. Chem. Int. Ed.* 60 (2021) 26725–26733, <https://doi.org/10.1002/anie.202110830>.
- [19] R.V. Ulijn, A.M. Smith, Designing peptide based nanomaterials, *Chem. Soc. Rev.* 37 (2008) 664, <https://doi.org/10.1039/b609047h>.
- [20] K. Matsui, Y. Segawa, K. Itami, All-benzene carbon nanocages: size-selective synthesis, photophysical properties, and crystal structure, *J. Am. Chem. Soc.* 136 (2014) 16452–16458, <https://doi.org/10.1021/ja509880v>.
- [21] N. Hayase, J. Nogami, Y. Shibata, K. Tanaka, Synthesis of a strained spherical carbon nanocage by regioselective alkyne cyclotrimerization, *Angew. Chem. Int. Ed.* 58 (2019) 9439–9442, <https://doi.org/10.1002/anie.201903422>.
- [22] E. Kayahara, T. Iwamoto, H. Takaya, T. Suzuki, M. Fujitsuka, T. Majima, N. Yasuda, N. Matsuyama, S. Seki, S. Yamago, Synthesis and physical properties of a ball-like three-dimensional  $\pi$ -conjugated molecule, *Nat. Commun.* 4 (2013) 2694, <https://doi.org/10.1038/ncomms3694>.
- [23] H. Sato, J.A. Bender, S.T. Roberts, M.J. Krische, Helical rod-like phenylene cages via ruthenium catalyzed diol-diene benzannulation: a cord of three strands, *J. Am. Chem. Soc.* 140 (2018) 2455–2459, <https://doi.org/10.1021/jacs.8b00131>.
- [24] S. Cui, G. Zhuang, D. Lu, Q. Huang, H. Jia, Y. Wang, S. Yang, P. Du, A three-dimensional capsule-like carbon nanocage as a segment model of capped zigzag [12,0] carbon nanotubes: synthesis, characterization, and complexation with C<sub>70</sub>, *Angew. Chem. Int. Ed.* 57 (2018) 9330–9335, <https://doi.org/10.1002/anie.201804031>.
- [25] T. Matsushima, S. Kikkawa, I. Azumaya, S. Watanabe, Triple helicene cage: three-dimensional  $\pi$ -conjugated chiral cage with six [5]Helicene units, *ChemistryOpen* 7 (2018) 278–281, <https://doi.org/10.1002/open.201800006>.
- [26] J. Song, N. Aratani, H. Shinokubo, A. Osuka, A porphyrin nanobarrel that encapsulates C<sub>60</sub>, *J. Am. Chem. Soc.* 132 (2010) 16356–16357, <https://doi.org/10.1021/ja107814s>.
- [27] Y. Wang, X.-S. Ke, S. Lee, S. Kang, V.M. Lynch, D.K. Kim, J.L. Sessler, Pyrene-bridged expanded carbaporphyrin nanobelts, *J. Am. Chem. Soc.* 144 (2022) 9212–9216, <https://doi.org/10.1021/jacs.2c01605>.
- [28] L. Ren, Y. Han, X. Hou, Y. Ni, J. Wu, All are aromatic: a 3D globally aromatic cage containing five types of 2D aromatic macrocycles, *Chem* 7 (2021) 3442–3453, <https://doi.org/10.1016/j.chempr.2021.11.003>.
- [29] Y. Ni, F. Gordillo-Gómez, M. Peña Alvarez, Z. Nan, Z. Li, S. Wu, Y. Han, J. Casado, J. Wu, A Chichibabin's hydrocarbon-based molecular cage: the impact of structural rigidity on dynamics, stability, and electronic properties, *J. Am. Chem. Soc.* 142 (2020) 12730–12742, <https://doi.org/10.1021/jacs.0c04876>.
- [30] D. Cui, F. Bai, L. Zhang, W. Li, Y. Zhang, K. Wang, M. Wu, C. Sun, H. Zang, B. Zou, X. Wang, Z. Su, Piezofluorochromism in hierarchical porous  $\pi$ -stacked supermolecular spring frameworks from aromatic chiral cages, *Angew. Chem. Int. Ed.* 63 (2024) e202319815, <https://doi.org/10.1002/anie.202319815>.
- [31] Y. Ge, Y. Hu, G. Duan, Y. Jin, W. Zhang, Advances and challenges in user-friendly alkyne metathesis catalysts, *Trends Chem.* 4 (2022) 540–553, <https://doi.org/10.1016/j.trechm.2022.03.004>.
- [32] C. Zhang, Q. Wang, H. Long, W. Zhang, A highly C<sub>70</sub> selective shape-persistent rectangular prism constructed through one-step alkyne metathesis, *J. Am. Chem. Soc.* 133 (2011) 20995–21001, <https://doi.org/10.1021/ja210418t>.
- [33] X. Yang, S. Huang, M. Ortiz, X. Wang, Y. Cao, O. Kareem, Y. Jin, F. Huang, X. Wang, W. Zhang, Truxene-based covalent organic polyhedrons constructed through alkyne metathesis, *Org. Chem. Front.* 8 (2021) 4723–4729, <https://doi.org/10.1039/D1QO00685A>.
- [34] M. Servalli, N. Trapp, M. Wörle, F.-G. Klärner, Anthraphane: an anthracene-based, propeller-shaped D<sub>3h</sub>-symmetric hydrocarbon cyclophane and its layered single crystal structures, *J. Organomet. Chem.* 81 (2016) 2572–2580, <https://doi.org/10.1021/acs.joc.6b00209>.
- [35] X. Gu, T.Y. Gopalakrishna, H. Phan, Y. Ni, T.S. Heng, J. Ding, J. Wu, A three-dimensionally  $\pi$ -conjugated diradical molecular cage, *Angew. Chem. Int. Ed.* 56 (2017) 15383–15387, <https://doi.org/10.1002/anie.201709537>.
- [36] D. Sakamaki, A. Ito, K. Tanaka, K. Furukawa, T. Kato, M. Shiro, 1,3,5-benzenetriamine double- and triple-Decker molecules, *Angew. Chem. Int. Ed.* 51 (2012) 8281–8285, <https://doi.org/10.1002/anie.201203451>.
- [37] J. Koo, I. Kim, Y. Kim, D. Cho, I.-C. Hwang, R.D. Mukhopadhyay, H. Song, Y. H. Ko, A. Dharmija, H. Lee, W. Hwang, S. Kim, M.-H. Baik, K. Kim, Gigantic porphyrinic cages, *Chem* 6 (2020) 3374–3384, <https://doi.org/10.1016/j.chempr.2020.10.002>.
- [38] H. Lee, J. Joo, A. Dharmija, A. Gunnam, J. Koo, P. Giri, Y. Ho Ko, I. Hwang, D. Kim, K. Kim, Flow synthesis of gigantic porphyrinic cages: facile synthesis of P<sub>12</sub>L<sub>24</sub> and discovery of kinetic product P<sub>6</sub>L<sub>18</sub>, *Chem. Eur. J.* 29 (2023) e202300760, <https://doi.org/10.1002/chem.202300760>.
- [39] S. Akine, M. Miyashita, S. Piao, T. Nabeshima, Perfect encapsulation of a guanidinium ion in a helical trnickel(II) metallocryptand for efficient regulation of the helix inversion rate, *Inorg. Chem. Front.* 1 (2014) 53–57, <https://doi.org/10.1039/C3QI00067B>.
- [40] S. Akine, M. Miyashita, T. Nabeshima, A metallo-molecular cage that can close the apertures with coordination bonds, *J. Am. Chem. Soc.* 139 (2017) 4631–4634, <https://doi.org/10.1021/jacs.7b00840>.
- [41] F. Aribot, A. Merle, P. Dechambenoit, H. Bock, A. Artigas, N. Vanthuyne, Y. Carissan, D. Hagebaum-Reignier, Y. Coquerel, F. Durola, A triply [5]Helicene-bridged (1,3,5)Cyclophane, *Angew. Chem. Int. Ed.* 62 (2023) e202304058, <https://doi.org/10.1002/anie.202304058>.
- [42] F. Qiu, X. Chen, W. Wang, K. Su, D. Yuan, Highly stable sp<sup>2</sup> carbon-conjugated porous organic cages, *CCS Chem.* 6 (2024) 149–156, <https://doi.org/10.31635/ccschem.023.202302903>.
- [43] P. Li, S. Xu, C. Yu, Z. Li, J. Xu, Z. Li, L. Zou, X. Leng, S. Gao, Z. Liu, X. Liu, S. Zhang, De novo construction of catenanes with dissymmetric cages by space-discriminative post-assembly modification, *Angew. Chem. Int. Ed.* 59 (2020) 7113–7121, <https://doi.org/10.1002/anie.202000442>.
- [44] D. Wang, L. Zhang, Y. Zhao, Template-free synthesis of an interlocked covalent organic molecular cage, *J. Organomet. Chem.* 87 (2022) 2767–2772, <https://doi.org/10.1021/acs.joc.1c02688>.
- [45] Y. Ni, T.Y. Gopalakrishna, H. Phan, T. Kim, T.S. Heng, Y. Han, T. Tao, J. Ding, D. Kim, J. Wu, 3D global aromaticity in a fully conjugated diradicaloid cage at different oxidation states, *Nat. Chem.* 12 (2020) 242–248, <https://doi.org/10.1038/s41557-019-0399-2>.
- [46] X.-S. Ke, T. Kim, Q. He, V.M. Lynch, D. Kim, J.L. Sessler, Three-dimensional fully conjugated carbaporphyrin cage, *J. Am. Chem. Soc.* 140 (2018) 16455–16459, <https://doi.org/10.1021/jacs.8b11158>.
- [47] O. El Bakouri, D.W. Szczepek, K. Jorner, R. Ayub, P. Bultinck, M. Solà, H. Ottosson, Three-dimensional fully  $\pi$ -conjugated macrocycles: when 3D-aromatic and when 2D-aromatic-in-3D? *J. Am. Chem. Soc.* 144 (2022) 8560–8575, <https://doi.org/10.1021/jacs.1c13478>.
- [48] S. Wu, Y. Ni, Y. Han, X. Hou, C. Wang, W. Hu, J. Wu, Hückel- and Baird-type global aromaticity in a 3D fully conjugated molecular cage, *Angew. Chem. Int. Ed.* 61 (2022) e202115571, <https://doi.org/10.1002/anie.202115571>.
- [49] S. Wu, Y. Ni, Y. Han, S. Xin, X. Hou, J. Zhu, Z. Li, J. Wu, Aromaticity in fully  $\pi$ -conjugated open-cage molecules, *J. Am. Chem. Soc.* 144 (2022) 23158–23167, <https://doi.org/10.1021/jacs.2c10859>.
- [50] G.-H. Ning, P. Cui, I.V. Sazanovich, J.T. Pegg, Q. Zhu, Z. Pang, R.-J. Wei, M. Towrie, K.E. Jelfs, M.A. Little, A.I. Cooper, Organic cage inclusion crystals exhibiting guest-enhanced multiphoton harvesting, *Chem* 7 (2021) 3157–3170, <https://doi.org/10.1016/j.chempr.2021.09.016>.
- [51] J. Kou, Q. Wu, D. Cui, Y. Geng, K. Zhang, M. Zhang, H. Zang, X. Wang, Z. Su, C. Sun, Selective encapsulation and chiral induction of C<sub>60</sub> and C<sub>70</sub> fullerenes by axially chiral porous aromatic cages, *Angew. Chem. Int. Ed.* 62 (2023) e202312733, <https://doi.org/10.1002/anie.202312733>.
- [52] H.-E. Högberg, B. Thulin, O. Wennerström, Bicyclophanehexaene, a new case cyclophane from a sixfold wittig reaction, *Tetrahedron Lett.* 18 (1977) 931–934, [https://doi.org/10.1016/S0040-4039\(01\)92795-9](https://doi.org/10.1016/S0040-4039(01)92795-9).
- [53] M. Servalli, N. Trapp, M. Solar, A.D. Schlüter, Library of single crystal structures of a D<sub>3h</sub>-symmetric hydrocarbon cyclophane: a comprehensive packing study of anthraphane from 30 solvents, *Cryst. Growth Des.* 17 (2017) 3419–3432, <https://doi.org/10.1021/acs.cgd.7b00367>.
- [54] M. Servalli, M. Solar, N. Trapp, M. Wörle, A.D. Schlüter, Photochemical single-crystal-to-single-crystal (SCSC) reactions of anthraphane to dianthraphane and poly 1D anthraphane, *Cryst. Growth Des.* 17 (2017) 6510–6522, <https://doi.org/10.1021/acs.cgd.7b01184>.
- [55] M. Servalli, N. Trapp, A.D. Schlüter, Single-crystal-to-single-crystal (SCSC) linear polymerization of a desymmetrized anthraphane, *Chem. Eur. J.* 24 (2018) 15003–15012, <https://doi.org/10.1002/chem.201802513>.
- [56] M. Servalli, L. Gyr, J. Sakamoto, A.D. Schlüter, Propeller-shaped D<sub>3h</sub>-symmetric macrocycles with three 1,8-diazaanthracene blades as building blocks for photochemically induced growth reactions, *Eur. J. Org. Chem.* 2015 (2015) 4519–4523, <https://doi.org/10.1002/ejoc.201500496>.
- [57] V. Boekelheide, R.A. Hollins, [2.2.2](1,3,5)Cyclophane and its derivatives. Extreme example of face-to-face crowding of aromatic rings, *J. Am. Chem. Soc.* 95 (1973) 3201–3208, <https://doi.org/10.1021/ja00791a023>.
- [58] A. Basavarajappa, M.D. Ambhore, V.G. Anand, Three dimensional isophlorinoid tetrapodal molecular cage, *Chem. Commun.* 57 (2021) 4299–4302, <https://doi.org/10.1039/D1CC01002F>.
- [59] K.D. Okochi, G.S. Han, I.M. Aldridge, Y. Liu, W. Zhang, Covalent assembly of heterosequenced macrocycles and molecular cages through orthogonal dynamic covalent chemistry (ODCC), *Org. Lett.* 15 (2013) 4296–4299, <https://doi.org/10.1021/ol4015283>.
- [60] K. Matsui, Y. Segawa, T. Namikawa, K. Kamada, K. Itami, Synthesis and properties of all-benzene carbon nanocages: a junction unit of branched carbon nanotubes, *Chem. Sci.* 4 (2013) 84–88, <https://doi.org/10.1039/C2SC21322B>.
- [61] F. Lucas, N. McIntosh, E. Jacques, C. Lebreton, B. Heinrich, B. Donnio, O. Jeanin, J. Rault-Berthelot, C. Quinton, J. Cornil, C. Poriel, [4]Cyclo-N-alkyl-2,7-carbazoles: influence of the alkyl chain length on the structural, electronic, and charge transport properties, *J. Am. Chem. Soc.* 143 (2021) 8804–8820, <https://doi.org/10.1021/jacs.1c03240>.
- [62] G.M. Peters, G. Grover, R.L. Maust, C.E. Colwell, H. Bates, W.A. Edgell, R. Jasti, M. Kertesz, J.D. Tovar, Linear and radial conjugation in extended  $\pi$ -Electron systems, *J. Am. Chem. Soc.* 142 (2020) 2293–2300, <https://doi.org/10.1021/jacs.9b10785>.
- [63] C.E. Colwell, T.W. Price, T. Stauch, R. Jasti, Strain visualization for strained macrocycles, *Chem. Sci.* 11 (2020) 3923–3930, <https://doi.org/10.1039/D0SC00629G>.

- [64] M. Iyoda, J. Yamakawa, M.J. Rahman, Conjugated macrocycles: concepts and applications, *Angew. Chem. Int. Ed.* 50 (2011) 10522–10553, <https://doi.org/10.1002/anie.201006198>.
- [65] S. Yamago, E. Kayahara, T. Iwamoto, Organoplatinum-mediated synthesis of cyclic  $\pi$ -conjugated molecules: towards a new era of three-dimensional aromatic compounds, *Chem. Rec.* 14 (2014) 84–100, <https://doi.org/10.1002/tcr.201300035>.
- [66] E. Kayahara, K. Fukuyama, T. Nishinaga, S. Yamago, Size dependence of [n]Cycloparaphenylenes ( $n = 5–12$ ) in electrochemical oxidation, *Chem. Asian J.* 11 (2016) 1793–1797, <https://doi.org/10.1002/asia.201600582>.
- [67] E.S. Hirst, R. Jasti, Bending benzene: syntheses of [n]Cycloparaphenylenes, *J. Organomet. Chem.* 77 (2012) 10473–10478, <https://doi.org/10.1021/jo302186h>.
- [68] X. Tian, R. Jasti, Cycloparaphenylenes: The shortest possible segments of armchair carbon nanotubes, in: M.A. Petrukhina, L.T. Scott (Eds.), *Fragments of Fullerenes and Carbon Nanotubes*, 1st ed., Wiley, 2011, pp. 291–309, <https://doi.org/10.1002/9781118011263.ch11>.
- [69] R. Jasti, C.R. Bertozzi, Progress and challenges for the bottom-up synthesis of carbon nanotubes with discrete chirality, *Chem. Phys. Lett.* 494 (2010) 1–7, <https://doi.org/10.1016/j.cplett.2010.04.067>.
- [70] L. Hu, Y. Guo, X. Yan, H. Zeng, J. Zhou, Electronic transport properties in [n]cycloparaphenylenes molecular devices, *Phys. Lett. A* 381 (2017) 2107–2111, <https://doi.org/10.1016/j.physleta.2017.04.035>.
- [71] J.B. Lin, E.R. Darzi, R. Jasti, I. Yavuz, K.N. Houk, Solid-state order and charge mobility in [5]- to [12]Cycloparaphenylenes, *J. Am. Chem. Soc.* 141 (2019) 952–960, <https://doi.org/10.1021/jacs.8b10699>.
- [72] M.R. Golder, R. Jasti, Syntheses of the smallest carbon nanostructures and the emergence of unique physical phenomena, *Acc. Chem. Res.* 48 (2015) 557–566, <https://doi.org/10.1021/acs.accounts.5b004253>.
- [73] E.J. Leonhardt, R. Jasti, Emerging applications of carbon nanostructures, *Nat. Rev. Chem.* 3 (2019) 672–686, <https://doi.org/10.1038/s41570-019-0140-0>.
- [74] E. Kayahara, V.K. Patel, S. Yamago, Synthesis and characterization of [5]Cycloparaphenylene, *J. Am. Chem. Soc.* 136 (2014) 2284–2287, <https://doi.org/10.1021/ja413214q>.
- [75] R. Jasti, J. Bhattacharjee, J.B. Neaton, C.R. Bertozzi, Synthesis, characterization, and theory of [9]-, [12]-, and [18]Cycloparaphenylene: carbon nanostructure, *J. Am. Chem. Soc.* 130 (2008) 17646–17647, <https://doi.org/10.1021/ja807126u>.
- [76] E. Kayahara, L. Sun, H. Onishi, K. Suzuki, T. Fukushima, A. Sawada, H. Kaji, S. Yamago, Gram-scale syntheses and conductivities of [10]Cycloparaphenylene and its tetraalkoxy derivatives, *J. Am. Chem. Soc.* 139 (2017) 18480–18483, <https://doi.org/10.1021/jacs.7b11526>.
- [77] S. Lee, E. Chénard, D.L. Gray, J.S. Moore, Synthesis of cycloparaphenyleneacetylene via alkyne metathesis: C<sub>70</sub> complexation and copper-free triple click reaction, *J. Am. Chem. Soc.* 138 (2016) 13814–13817, <https://doi.org/10.1021/jacs.6b08752>.
- [78] X. Zhou, R.R. Thompson, F.R. Fronczek, S. Lee, Size-selective synthesis of large cycloparaphenyleneacetylene carbon nanostructures using alkyne metathesis, *Org. Lett.* 21 (2019) 4680–4683, <https://doi.org/10.1021/acs.orglett.9b01563>.
- [79] D. Lu, S. Cui, P. Du, Large  $\pi$ -extension of carbon nanorings by incorporating Hexa-peri-hexabenzocoronenes, *Synlett* 28 (2017) 1671–1677, <https://doi.org/10.1055/s-0036-1588830>.
- [80] J. Xia, R. Jasti, Synthesis, characterization, and crystal structure of [6]Cycloparaphenylene, *Angew. Chem. Int. Ed.* 51 (2012) 2474–2476, <https://doi.org/10.1002/anie.201108167>.
- [81] M.A. Majewski, M. Stepien, Schalen, Reifen und Sattel: methoden zur synthese gebogener aromatischer Moleküle, *Angew. Chem.* 131 (2019) 90–122, <https://doi.org/10.1002/ange.201807004>.
- [82] E. Kayahara, T. Iwamoto, T. Suzuki, S. Yamago, Selective synthesis of [6]-, [8]-, and [10]Cycloparaphenylenes, *Chem. Lett.* 42 (2013) 621–623, <https://doi.org/10.1246/cl.130188>.
- [83] P.J. Stang, D.H. Cao, Transition metal based cationic molecular boxes. Self-assembly of macrocyclic platinum(II) and palladium(II) tetranuclear complexes, *J. Am. Chem. Soc.* 116 (1994) 4981–4982, <https://doi.org/10.1021/ja00090a051>.
- [84] M. Fujita, J. Yazaki, K. Ogura, Preparation of a macrocyclic polynuclear complex, [(en)Pd(4,4'-bpy)]<sub>4</sub>(NO<sub>3</sub>)<sub>8</sub> (en = ethylenediamine, bpy = bipyridine), which recognizes an organic molecule in aqueous media, *J. Am. Chem. Soc.* 112 (1990) 5645–5647, <https://doi.org/10.1021/ja00170a042>.
- [85] L. Sturm, F. Aribot, L. Soliman, H. Bock, F. Durola, The Perkin strategy for the synthesis of large Carboxy-substituted polycyclic aromatic compounds, *Eur. J. Org. Chem.* 2022 (2022) e202200196, <https://doi.org/10.1002/ejoc.202200196>.
- [86] G. Naulet, A. Robert, P. Dechambenoit, H. Bock, F. Durola, Monoprotection of arylene-diacetic acids allowing the build-up of longer aromatic ribbons by successive Perkin condensations, *Eur. J. Org. Chem.* 2018 (2018) 619–626, <https://doi.org/10.1002/ejoc.201701499>.
- [87] A. Robert, P. Dechambenoit, H. Bock, F. Durola, A carboxyfunctionalized (2,4)-1,6-pyrenophane-tetraene by glyoxylic Perkin condensation, *Can. J. Chem.* 95 (2017) 450–453, <https://doi.org/10.1139/cjc-2016-0585>.
- [88] H. Bock, D. Subervie, P. Mathey, A. Pradhan, P. Sarkar, P. Dechambenoit, E. A. Hillard, F. Durola, Helicenes from diarylmalimides, *Org. Lett.* 16 (2014) 1546–1549, <https://doi.org/10.1021/ol500154k>.
- [89] H. Sato, M.A. Blemker, G. Hellinghausen, D.W. Armstrong, J.W. Nafie, S. T. Roberts, M.J. Krische, Triple helical Ir(ppy)<sub>3</sub> phenylene cage prepared by diol-mediated benzannulation: synthesis, resolution, absolute stereochemistry and photophysical properties, *Chem. Eur. J.* 25 (2019) 8719–8724, <https://doi.org/10.1002/chem.201902122>.
- [90] J. Song, N. Aratani, J.H. Heo, D. Kim, H. Shinokubo, A. Osuka, Directly Pd(II)-bridged porphyrin belts with remarkable curvatures, *J. Am. Chem. Soc.* 132 (2010) 11868–11869, <https://doi.org/10.1021/ja1046654>.
- [91] M.D. Peeks, T.D.W. Claridge, H.L. Anderson, Aromatic and antiaromatic ring currents in a molecular nanoring, *Nature* 541 (2017) 200–203, <https://doi.org/10.1038/nature20798>.
- [92] T. Tanaka, A. Osuka, Chemistry of meso-aryl-substituted expanded porphyrins: aromaticity and molecular twist, *Chem. Rev.* 117 (2017) 2584–2640, <https://doi.org/10.1021/acs.chemrev.6b00371>.
- [93] M. Rickhaus, M. Jirasek, L. Tejerina, H. Gotfredsen, M.D. Peeks, R. Haver, H.-W. Jiang, T.D.W. Claridge, H.L. Anderson, Global aromaticity at the nanoscale, *Nat. Chem.* 12 (2020) 236–241, <https://doi.org/10.1038/s41557-019-0398-3>.
- [94] P. Von Ragué Schleyer, H. Jiao, B. Goldfuss, P.K. Freeman, Aromaticity and antiaromaticity in five-membered C<sub>4</sub>H<sub>4</sub> X ring systems: “Classical” and “Magnetic” concepts may not be “Orthogonal”, *Angew. Chem. Int. Ed. Eng.* 34 (1995) 337–340, <https://doi.org/10.1002/anie.199503371>.
- [95] A.R. Katritzky, K. Jug, D.C. Oniciu, Quantitative measures of aromaticity for mono-, bi-, and tricyclic penta- and hexatomic heteroaromatic ring systems and their interrelationships, *Chem. Rev.* 101 (2001) 1421–1450, <https://doi.org/10.1021/cr990327m>.
- [96] C. Yu, H. Long, Y. Jin, W. Zhang, Synthesis of cyclic porphyrin trimers through alkyne metathesis cyclooligomerization and their host-guest binding study, *Org. Lett.* 18 (2016) 2946–2949, <https://doi.org/10.1021/acs.orglett.6b01293>.
- [97] J. Oh, Y.M. Sung, H. Mori, S. Park, K. Jorner, H. Ottosson, M. Lim, A. Osuka, D. Kim, Unraveling excited-singlet-state aromaticity via vibrational analysis, *Chem* 3 (2017) 870–880, <https://doi.org/10.1016/j.chempr.2017.09.005>.
- [98] W.-Y. Cha, T. Kim, A. Ghosh, Z. Zhang, X.-S. Ke, R. Ali, V.M. Lynch, J. Jung, W. Kim, S. Lee, S. Fukuzumi, J.S. Park, J.L. Sessler, T.K. Chandrashekar, D. Kim, Bicyclic Baird-type aromaticity, *Nat. Chem.* 9 (2017) 1243–1248, <https://doi.org/10.1038/nchem.2834>.
- [99] R. Nozawa, J. Kim, J. Oh, A. Lamping, Y. Wang, S. Shimizu, I. Hisaki, T. Kowalczyk, H. Fliegl, D. Kim, H. Shinokubo, Three-dimensional aromaticity in an antiaromatic cyclophane, *Nat. Commun.* 10 (2019) 3576, <https://doi.org/10.1038/s41467-019-11467-4>.
- [100] B.K. Reddy, J. Rawson, S.C. Gadekar, P. Kögerler, V.G. Anand, A naphthalene-fused dimer of an anti-aromatic expanded isophlorin, *Chem. Commun.* 53 (2017) 8211–8214, <https://doi.org/10.1039/C7CC04050D>.
- [101] L.K. Montgomery, J.C. Huffman, E.A. Jurczak, M.P. Grendze, The molecular structures of Thiele’s and Chichibabin’s hydrocarbons, *J. Am. Chem. Soc.* 108 (1986) 6004–6011, <https://doi.org/10.1021/ja00279a056>.
- [102] S. Dong, Z. Tong, Y. Han, J. Wang, J. Zhang, A. Li, T.Y. Gopalakrishna, H. Tian, C. Chi, Facile synthesis and characterization of Aza-bridged all-benzenoid quinoidal figure-eight and cage molecules, *Chem. Sci.* 15 (2024) 9087–9095, <https://doi.org/10.1039/D3SC02070D>.
- [103] T. Tozawa, J.T.A. Jones, S.I. Swamy, S. Jiang, D.J. Adams, S. Shakespeare, R. Clowes, D. Bradshaw, T. Hasell, S.Y. Chong, C. Tang, S. Thompson, J. Parker, A. Trewin, J. Bacsa, A.M.Z. Slawin, A. Steiner, A.I. Cooper, Porous organic cages, *Nat. Mater.* 8 (2009) 973–978, <https://doi.org/10.1038/nmat2545>.
- [104] Y. Jin, B.A. Voss, R.D. Noble, W. Zhang, A shape-persistent organic molecular cage with high selectivity for the adsorption of CO<sub>2</sub> over N<sub>2</sub>, *Angew. Chem. Int. Ed.* 49 (2010) 6348–6351, <https://doi.org/10.1002/anie.201001517>.
- [105] Y. Jin, B.A. Voss, A. Jin, H. Long, R.D. Noble, W. Zhang, Highly CO<sub>2</sub>-selective organic molecular cages: what determines the CO<sub>2</sub> selectivity, *J. Am. Chem. Soc.* 133 (2011) 6650–6658, <https://doi.org/10.1021/ja110846c>.
- [106] M.E. Belowich, J.F. Stoddart, Dynamic imine chemistry, *Chem. Soc. Rev.* 41 (2012) 2003–2024, <https://doi.org/10.1039/C2CS15305J>.
- [107] G. Zhang, M. Mastalerz, Organic cage compounds – from shape-persistence to function, *Chem. Soc. Rev.* 43 (2014) 1934–1947, <https://doi.org/10.1039/C3CS60358J>.
- [108] S. Hong, Md.R. Rohman, J. Jia, Y. Kim, D. Moon, Y. Kim, Y.H. Ko, E. Lee, K. Kim, Porphyrin boxes: rationally designed porous organic cages, *Angew. Chem. Int. Ed.* 54 (2015) 13241–13244, <https://doi.org/10.1002/anie.201505531>.
- [109] T. Hasell, A.I. Cooper, Porous organic cages: soluble, modular and molecular pores, *Nat. Rev. Mater.* 1 (2016) 16053, <https://doi.org/10.1038/natrevmats.2016.53>.
- [110] M. Mastalerz, Porous shape-persistent organic cage compounds of different size, geometry, and function, *Acc. Chem. Res.* 51 (2018) 2411–2422, <https://doi.org/10.1021/acs.accounts.8b00298>.
- [111] H. Wang, Y. Jin, N. Sun, W. Zhang, J. Jiang, Post-synthetic modification of porous organic cages, *Chem. Soc. Rev.* 50 (2021) 8874–8886, <https://doi.org/10.1039/D0CS01142H>.
- [112] P. Bhandari, P.S. Mukherjee, Post-synthesis conversion of an unstable imine cage to a stable cage with amide moieties towards selective receptor for furine cage, *Chem. Eur. J.* 28 (2022) e202201901, <https://doi.org/10.1002/chem.202201901>.
- [113] P. Alexandre, W. Zhang, F. Rominger, S.M. Elbert, R.R. Schröder, M. Mastalerz, A robust porous quinoline cage: transformation of a [4+6] salicylimine cage by Povarov cyclization, *Angew. Chem. Int. Ed.* 59 (2020) 19675–19679, <https://doi.org/10.1002/anie.202007048>.
- [114] X.-Y. Hu, W.-S. Zhang, F. Rominger, I. Wacker, R.R. Schröder, M. Mastalerz, Transforming a chemically labile [2+3] imine cage into a robust carbamate cage, *Chem. Commun.* 53 (2017) 8616–8619, <https://doi.org/10.1039/C7CC03677A>.

- [115] T.H.G. Schick, J.C. Lauer, F. Rominger, M. Mastalerz, Transformation of imine cages into hydrocarbon cages, *Angew. Chem. Int. Ed.* 58 (2019) 1768–1773, <https://doi.org/10.1002/anie.201814243>.
- [116] S.J. Rowan, S.J. Cantrill, G.R.L. Cousins, J.K.M. Sanders, J.F. Stoddart, Dynamic covalent chemistry, *Angew. Chem. Int. Ed.* 41 (2002) 898–952, [https://doi.org/10.1002/1521-3773\(20020315\)41:6<898::AID-ANIE898>3.0.CO;2-E](https://doi.org/10.1002/1521-3773(20020315)41:6<898::AID-ANIE898>3.0.CO;2-E).
- [117] M. Mastalerz, Shape-persistent organic cage compounds by dynamic covalent bond formation, *Angew. Chem. Int. Ed.* 49 (2010) 5042–5053, <https://doi.org/10.1002/anie.201000443>.
- [118] N.M. Rue, J. Sun, R. Warmuth, Polyimine container molecules and nanocapsules, *Isr. J. Chem.* 51 (2011) 743–768, <https://doi.org/10.1002/ijch.201100064>.
- [119] Y. Jin, Y. Zhu, W. Zhang, Development of organic porous materials through Schiff-base chemistry, *CrystEngComm* 15 (2013) 1484–1499, <https://doi.org/10.1039/C2CE26394G>.
- [120] Y. Jin, C. Yu, R.J. Denman, W. Zhang, Recent advances in dynamic covalent chemistry, *Chem. Soc. Rev.* 42 (2013) 6634, <https://doi.org/10.1039/c3cs60044k>.
- [121] F.M. Akwi, P. Watts, Continuous flow chemistry: where are we now? Recent applications, challenges and limitations, *Chem. Commun.* 54 (2018) 13894–13928, <https://doi.org/10.1039/C8CC07427E>.
- [122] Y. Yang, C. Schäfer, K. Börjesson, Detachable all-carbon-linked 3D covalent organic framework films for semiconductor/COF heterojunctions by continuous flow synthesis, *Chem* 8 (2022) 2217–2227, <https://doi.org/10.1016/j.chempr.2022.05.003>.
- [123] J. Zhu, Y. Han, Y. Ni, S. Wu, Q. Zhang, T. Jiao, Z. Li, J. Wu, Facile synthesis of a fully fused, three-dimensional  $\pi$ -conjugated Archimedean cage with magnetically shielded cavity, *J. Am. Chem. Soc.* 143 (2021) 14314–14321, <https://doi.org/10.1021/jacs.1c06490>.
- [124] Z.U. Levi, T.D. Tilley, Synthesis and electronic properties of extended, fused-ring aromatic systems containing multiple pentalene units, *J. Am. Chem. Soc.* 132 (2010) 11012–11014, <https://doi.org/10.1021/ja1043159>.
- [125] J. Zhu, Y. Han, Y. Ni, G. Li, J. Wu, Facile synthesis of nitrogen-doped [(6, $n$ ), 8] $_n$  cyclacene carbon nanobelts by a one-pot self-condensation reaction, *J. Am. Chem. Soc.* 143 (2021) 2716–2721, <https://doi.org/10.1021/jacs.1c00409>.
- [126] A.Q. Ramlle, E.R.T. Tiekink, Synthetic strategies and diversification of dibenzo [1,5]diazocines, *Org. Biomol. Chem.* 21 (2023) 2870–2888, <https://doi.org/10.1039/D3OB00192J>.
- [127] M. Takeda, S. Hiroto, H. Yokoi, S. Lee, D. Kim, H. Shinokubo, Azabuckybowl-based molecular tweezers as C<sub>60</sub> and C<sub>70</sub> receptors, *J. Am. Chem. Soc.* 140 (2018) 6336–6342, <https://doi.org/10.1021/jacs.8b02327>.
- [128] A. Sacristán-Martín, D. Miguel, A. Diez-Varga, H. Barbero, C.M. Álvarez, From induced-fit assemblies to ternary inclusion complexes with fullerenes in corannulene-based molecular tweezers, *J. Organomet. Chem.* 87 (2022) 16691–16706, <https://doi.org/10.1021/acs.joc.2c02345>.
- [129] E. Misselwitz, J. Spengler, F. Rominger, M. Kivala, Indenoannulated tridecacyclene: an all-carbon seven-stage redox-amphoter, *Chem. Eur. J.* 30 (2024) e202400696, <https://doi.org/10.1002/chem.202400696>.
- [130] Z.-L. Qiu, Y. Cheng, Q. Zeng, Q. Wu, X.-J. Zhao, R.-J. Xie, L. Feng, K. Liu, Y.-Z. Tan, Synthesis and interlayer assembly of a graphenic bowl with peripheral selenium annulation, *J. Am. Chem. Soc.* 145 (2023) 3289–3293, <https://doi.org/10.1021/jacs.2c12401>.
- [131] A.R. Sanford, L. Yuan, W. Feng, K. Yamato, R.A. Flowers, B. Gong, Cyclic aromatic oligoamides as highly selective receptors for the guanidinium ion, *Chem. Commun.* (2005) 4720–4722, <https://doi.org/10.1039/b504411a>.
- [132] A. Giacomelli, C. Floriani, G. Perego, Guanidinium and alkylammonium ion complexation by Nickel(II) Schiff base complexes, *J. Chem. Soc. Chem. Commun.* (1982) 650–652, <https://doi.org/10.1039/C39820000650>.
- [133] K.D. Okochi, Y. Jin, W. Zhang, Highly efficient one-pot synthesis of hetero-sequenced shape-persistent macrocycles through orthogonal dynamic covalent chemistry (ODCC), *Chem. Commun.* 49 (2013) 4418–4420, <https://doi.org/10.1039/C2CC33078D>.
- [134] G.C. Vougioukalakis, R.H. Grubbs, Ruthenium-based heterocyclic carbene-coordinated olefin metathesis catalysts, *Chem. Rev.* 110 (2010) 1746–1787, <https://doi.org/10.1021/cr900242a>.
- [135] P. Compain, Olefin metathesis of amine-containing systems: beyond the current consensus, *Adv. Synth. Catal.* 349 (2007) 1829–1846, <https://doi.org/10.1002/adsc.200700161>.
- [136] G.O. Wilson, K.A. Porter, H. Weissman, S.R. White, N.R. Sottos, J.S. Moore, Stability of second generation Grubbs' alkylidenes to primary amines: formation of novel ruthenium-amine complexes, *Adv. Synth. Catal.* 351 (2009) 1817–1825, <https://doi.org/10.1002/adsc.200900134>.
- [137] Z. Wu, S. Lee, J.S. Moore, Synthesis of three-dimensional nanoscaffolding, *J. Am. Chem. Soc.* 114 (1992) 8730–8732, <https://doi.org/10.1021/ja00048a073>.
- [138] S. Lee, A. Yang, T.P. Money Penny, J.S. Moore, Kinetically trapped tetrahedral cages via alkyne metathesis, *J. Am. Chem. Soc.* 138 (2016) 2182–2185, <https://doi.org/10.1021/jacs.6b00468>.
- [139] T.P.M. Ii, A. Yang, N.P. Walter, T.J. Woods, D.L. Gray, Y. Zhang, J.S. Moore, Product distribution from precursor bite angle variation in multitopic alkyne metathesis: evidence for a putative kinetic bottleneck, *J. Am. Chem. Soc.* 140 (2018) 5825–5833, <https://doi.org/10.1021/jacs.8b02184>.
- [140] Q. Wang, C. Zhang, B.C. Noll, H. Long, Y. Jin, W. Zhang, A tetrameric cage with D<sub>2h</sub> symmetry through alkyne metathesis, *Angew. Chem. Int. Ed.* 53 (2014) 10663–10667, <https://doi.org/10.1002/anie.201404880>.
- [141] Q. Wang, C. Yu, C. Zhang, H. Long, S. Azarmoush, Y. Jin, W. Zhang, Dynamic covalent synthesis of arylenethynylene cages through alkyne metathesis: dimer, tetramer, or interlocked complex? *Chem. Sci.* 7 (2016) 3370–3376, <https://doi.org/10.1039/C5SC04977F>.
- [142] Q. Wang, C. Yu, H. Long, Y. Du, Y. Jin, W. Zhang, Solution-phase dynamic assembly of permanently interlocked arylenethynylene cages through alkyne metathesis, *Angew. Chem. Int. Ed.* 54 (2015) 7550–7554, <https://doi.org/10.1002/anie.201501679>.
- [143] C.C. Pattillo, J.S. Moore, A tetrahedral molecular cage with a responsive vertex, *Chem. Sci.* 10 (2019) 7043–7048, <https://doi.org/10.1039/C9SC02047K>.
- [144] S. Huang, Z. Lei, Y. Jin, W. Zhang, By-design molecular architectures via alkyne metathesis, *Chem. Sci.* 12 (2021) 9591–9606, <https://doi.org/10.1039/D1SC01881G>.
- [145] W. Bai, W. Wei, H.H.Y. Sung, I.D. Williams, Z. Lin, G. Jia, Syntheses of Re(V) alkylidyne complexes and ligand effect on the reactivity of Re(V) alkylidyne complexes toward alkynes, *Organometallics* 37 (2018) 559–569, <https://doi.org/10.1021/acs.organomet.7b00877>.
- [146] H. Yang, Z. Liu, W. Zhang, Multidentate triphenylsilane-based alkyne metathesis catalysts, *Adv. Synth. Catal.* 355 (2013) 885–890, <https://doi.org/10.1002/adsc.201201105>.
- [147] J. Luo, T. Lei, X. Xu, F. Li, Y. Ma, K. Wu, J. Pei, Three-dimensional shape-persistent fluorescent nanocages: facile dynamic synthesis, photophysical properties, and surface morphologies, *Chem. Eur. J.* 14 (2008) 3860–3865, <https://doi.org/10.1002/chem.200800154>.
- [148] X.-Y. Cao, W.-B. Zhang, J.-L. Wang, X.-H. Zhou, H. Lu, J. Pei, Extended  $\pi$ -conjugated dendrimers based on truxene, *J. Am. Chem. Soc.* 125 (2003) 12430–12431, <https://doi.org/10.1021/ja037723d>.
- [149] S. Séjourmé, A. Labrunie, C. Dalinot, A. Benchohra, V. Carré, F. Aubriet, M. Allain, M. Sallé, S. Goeb, Chiral self-sorting in truxene-based metallacages, *Inorganics* 8 (2019) 1, <https://doi.org/10.3390/inorganics8010001>.
- [150] X. Wang, Y. Wang, H. Yang, H. Fang, R. Chen, Y. Sun, N. Zheng, K. Tan, X. Lu, Z. Tian, X. Cao, Assembled molecular face-rotating polyhedra to transfer chirality from two to three dimensions, *Nat. Commun.* 7 (2016) 12469, <https://doi.org/10.1038/ncomms12469>.
- [151] D. Sakamaki, A. Ito, K. Furukawa, T. Kato, K. Tanaka, High-spin polycationic states of an alternate meta-para-linked oligoarylamine incorporating two macrocycles, *Chem. Commun.* (2009) 4524–4526, <https://doi.org/10.1039/B907792H>.
- [152] B. Narymbetov, A. Omerzu, V.V. Kabanov, M. Tokumoto, H. Kobayashi, D. Mihailovic, Origin of ferromagnetic exchange interactions in a fullerene-organic compound, *Nature* 407 (2000) 883–885, <https://doi.org/10.1038/35038032>.
- [153] A. Ito, Y. Yamagishi, K. Fukui, S. Inoue, Y. Hirao, K. Furukawa, T. Kato, K. Tanaka, Trimacrocyclic arylamine and its polycationic states, *Chem. Commun.* (2008) 6573–6575, <https://doi.org/10.1039/b816311a>.